Infrared Satellite-Derived Sea Surface Skin Temperature Sensitivity to Aerosol Vertical Distribution − Field Data Analysis and Model Simulations

Submitted to SPECIAL SECTION on the "Terra Mission - 20 Years of Science"

Bingkun Luo, Peter J. Minnett
Rosenstiel School of Marine and Atmospheric Science
University of Miami
4600 Rickenbacker Causeway
Miami, FL 33149

&

Nicholas R. Nalli
IMSG, Inc. at National Oceanic and Atmospheric Administration (NOAA)
NESDIS/STAR, College Park, MD 20740

Corresponding Author:
Bingkun Luo
Meteorology and Physical Oceanography Program
Rosenstiel School of Marine and Atmospheric Science
University of Miami
4600 Rickenbacker Causeway
Miami, FL 33149-1031, USA

Tel: +1 (305) 333-5688
email: LBK@rsmas.miami.edu

Abstract

Sea surface temperature is an Essential Climate Variable. The radiative impact of mineral dust is one of the major contributors to inaccuracies in the satellite-retrieved sea surface skin temperature (SST_{skin}). Different aerosol dust vertical distributions have varying effects on the satellite-derived SST_{skin}. To further investigate the physical mechanisms of aerosol effects on Terra MODerate-resolution Imaging Spectroradiometers (MODIS) derived SST_{skin}, the aerosol radiative effects were studied with a field-data match-up analysis and radiative transfer simulations. The field data are measurements of the SST_{skin} derived from highly accurate ship-based infrared spectrometers vertical atmospheric temperature and water vapor radiosonde profiles. The aerosol dust concentrations in three-dimensions from the NASA Modern-Era Retrospective analysis for Research and Applications, Version 2 have been used as input to radiative transfer simulations. Based on the analysis of field data and simulations, we have empirically determined that the sensitivity of the Terra MODIS retrieved SST_{skin} accuracies is related to 1) dust concentration in the atmosphere, 2) the dust layer altitude, and 3) the dust layer temperature. As the aerosol altitude increases, the effect on the SST_{skin} retrievals becomes more negative in proportion to the temperature contrast with the sea surface. SST_{skin} differences, satellite-derived - surface measurements, for a given aerosol layer optical depth vary between -3 K and 1 K according to our match-up comparisons and radiative transfer simulations.

Submitted to SPECIAL SECTION on the "Terra Mission - 20 Years of Science"

1. Introduction

Sea-surface temperature (SST) is a major governing factor in air-sea exchanges of heat, moisture, gases and momentum; it also indicates surface circulation patterns in the upper ocean. Infrared imaging radiometers on polar orbiting, earth-observation satellites have provided measurements for the retrieval of SST for a half-century (Minnett et al. 2019). Starting with the High Resolution Infrared Radiometer (HRIR) on the NASA satellite Nimbus-1 (Allison and Kennedy 1967; Smith et al. 1970) and through a series of Advanced Very High Resolution Radiometers (AVHRR, Cracknell (1997)), satellite SST retrievals have played a significant role in generating time series of quantitative estimates of SST (Kilpatrick et al. 2001; Merchant et al. 2019; Reynolds and Smith 1994). TERRA was launched in December 1999 with a descending (from north to south) equatorial crossing local time of 10:30 a.m. ± 5 minutes (Xiong et al. 2008a). TERRA was developed to pair with another EOS (Earth Observing System) satellite – AQUA – which was launched in May 2002 into an orbit with an ascending node (from south to north) equatorial crossing local time of around 13:30 p.m. Both satellites carry several instruments to investigate the Earth's atmosphere and surface. Over the past twenty years, the Moderate Resolution Imaging Spectroradiometer (MODIS; Esaias et al. (1998)) onboard TERRA has taken nearly continuous measurements for more than 108,000 orbits, with an unprecedented spectral resolution, while sampling the Earth's surface and atmosphere. The missions of the AVHRR and MODIS are being extended in the USA by the Visible Infrared Imaging Radiometer Suite (VIIRS; Schueler et al. (2013)) onboard the Suomi-National Polar-orbiting Partnership satellite (S-NPP) and NOAA20, with further VIIRS to be flown on future NOAA polar-orbiting satellites (Minnett et al. 2020).

Radiometers on European satellites, such as the Sea and Land Surface Temperature Radiometer (SLSTR; Merchant (2012); Donlon et al. (2012)) and the METimage (Schmülling et al. 2010; Wallner et al. 2017), will also extend the SST record from polar-orbiting satellites. These, and other infrared satellite instruments have provided other atmospheric and oceanic data for use in weather forecasting and in operational oceanography, and for studying the climate system. These satellite missions and applications will continue into the foreseeable future (Minnett et al. 2019).

Definitions of various kinds of SST were introduced by the Group for High Resolution SST (GHRSST; Donlon et al. (2007)) according to the thermal variability of the upper ocean. The infrared radiometer derived temperature is usually characteristic of a depth of less than 1 mm, determined by the emission depth of the infrared radiation (Bertie and Lan 1996; Donlon et al. 2014b; Downing and Williams 1975; Hale and Querry 1973; Judd and Handler 2019). During daytime the temperature variability is influenced by absorbing solar radiation, modulated by cloud cover, as well as by losing heat to the atmosphere, the latter being dependent on surface wind and surface-driven turbulence and occurring during both daytime and nighttime (Gentemann et al. 2009; Minnett 2003). More detailed discussions of near-surface SST are given by Donlon et al. (2007) and Minnett and Kaiser-Weiss (2012).

Sea surface skin temperature (SST_{skin}) retrievals from infrared measurements from satellites are taken in relatively transparent atmospheric "windows." The atmospheric transmissivity is very variable, mainly due to variations in the atmospheric water vapor distribution, being ~0.98 across the λ = 10-13 μm window for cold, dry Arctic atmospheres, but being reduced for moist, tropical marine atmospheres to ~0.35 at λ = 11 μm and ~0.23 at λ = 12 μm. These transmissivities are for vertical propagation through the atmosphere, and are further reduced for propagation of the radiation along longer slant-paths at non-zero zenith angles. The most common approaches to correct for the radiative effects of the intervening atmospheres are based on measurements in spectral bands at wavelengths close to 3.7 μm, 11 μm and 12 μm, where the atmospheric transmissivity has a spectral dependence. Measurements in the shorter wavelength spectral intervals in the 3.5-4.1μm range are contaminated during the daytime by reflected sun glint at the surface or scattered solar radiation within the atmosphere; they have generally been used during nighttime. The limited number of infrared window channels in a single view has long been recognized as having insufficient information content to permit the correction of the effects of aerosol variability as well as the full range of air temperature and water vapor variability and air-sea temperature differences (Merchant et al. 2006; Walton 2016). SST_{skin} retrievals depend on the algorithms being suitable for the tasks; the errors and uncertainties of the derived variables being confidently estimated, and the dependencies of estimated retrieval errors and uncertainties on controlling parameters such as aerosol dust being well understood.

The attenuation of the upward-propagating surface infrared emission due to aerosol dust has been studied extensively. For example, Nalli et al. (2012) and Nalli et al. (2013) discussed the angular effects of aerosols in clear-sky radiance measurements, and derived a simple physical conceptual model to quantify the infrared brightness temperature sensitivity to aerosols and residual clouds that were not correctly identified by cloud screening algorithms (Kilpatrick et al. 2019). The brightness temperatures derived from measurements at satellite height are affected by the radiative path through the dust layer, its shape and vertical concentration distribution, and temperature contrast between the dust layer and sea surface. Building on earlier results which indicated poorer accuracies of AVHRR-derived SST due to aerosols (Díaz et al. 2001), Arbelo et al. (2003) reported a relationship between AVHRR-derived SST errors and aerosols by comparisons with temperatures measured from satellites and drifting buoys in the area of the Atlantic Ocean where Saharan dust outbreaks occur. The impact of aerosols on the SST_{skin} retrievals from measurements of the Along-Track Scanning Radiometers (ATSR) are much reduced because of the dual-view scan mechanism (Brown et al. 1997; O'Carroll et al. 2012), whereas the SST_{skin} retrievals of the linear-scanning AVHRR are very susceptible to the effects of desert aerosol dust. Vázquez-Cuervo et al. (2004) found the differences between ATSR-2 and AVHRR SST retrievals varied regionally, being most significant in the Sahara dust region. Luo et al. (2020a) found that SLSTR (Merchant 2012) SST_{skin} retrievals could be affected by Sahara aerosol dusts. Aerosol optical depth (AOD) is a measure of the aerosol concentration in the atmosphere derived by integrating the aerosol attenuation coefficient along the propagation path. Bogdanoff et al. (2015) demonstrated the sensitivity of AVHRR SST retrievals to the vertical distribution of aerosol dust layers using a radiative-transfer model: the error was found to be over 1 K for 0.25 AOD and concluded that the dust layer thermal infrared influence at various heights should be considered when attempting to improve the accuracy of infrared satellite SST retrievals.

Aerosol particles absorb, scatter and emit infrared radiation; thus, the satellite-measured radiation at the top of the atmosphere should be corrected for these effects before an unbiased SST_{skin} can be derived. Efforts to establish a scheme to minimize the errors due to aerosols have been made for many years (Blackmore et al. 2012; Marullo et al. 2010). Nalli and Stowe (2002) presented a daytime dust correction method for AVHRR onboard NOAA satellites, in which the reflectance ratio between AVHRR channel 1 (λ = 0.58 to 0.68 μm) and channel 2 (λ = 0.75 to 1.1 μm) was sensitive to the AOD. The empirically derived aerosol correction method was shown to reduce notably the SST differences with respect to buoy observations. Merchant et al. (2006) proposed the Saharan Dust Index (SDI) as a result of analysis of radiative transfer model simulations of the measurements of the Spinning Enhanced Visible and InfraRed Imager (SEVIRI), SDI is used to correct the SST retrieval algorithms with an empirical expression; the results showed an average of 0.2 K error was removed for SEVIRI SST retrievals; and Le Borgne et al. (2013) used the same method for VIIRS onboard S-NPP, the standard deviation was reduced by an amount in the range of 0.1 K to 0.15 K for VIIRS. For the Along-Track Scanning Radiometers (ATSRs), Good et al. (2012) derived the ATSR Saharan dust index (ASDI) with the principal component analysis of the brightness temperature differences of selected channels; the second principal component was related to AOD and can be used to effectively detect the mineral dust. More recently, Luo et al. (2019) developed a night-time Dust-induced SST Difference Index (DSDI) for MODIS onboard the AQUA satellite; the average SST differences were reduced by 0.16 K near Saharan dust regions, dependent on the MODIS data quality level.

Radiative transfer simulations of the SST_{skin} errors show they are related to the dust layer temperature and altitude; the SST_{skin} errors are directly attributable to the aerosol dust influence on the satellite brightness temperatures. Following Nalli et al. (2012), the infrared brightness temperature change δT_{Ba} due to aerosol dust optical depth

$\tau_{\lambda a}$ for an idealized "super window" (an idealized super-transparent micro-window with negligible attenuation by gases) can be theoretically written as

$$\delta T_{Ba}(\lambda, \theta, \tau_{\lambda a}, T_s, \bar{T}_a) \approx [1 - \exp(-\tau_{\lambda a}\sec\theta)] \frac{\left[\frac{\partial B_\lambda}{\partial T}\right]_{\bar{T}_{Sa}}}{\left[\frac{\partial B_\lambda}{\partial T}\right]_{\bar{T}_B}} \delta T_{sa} \qquad \text{Equation (1)}$$

where δT_{Ba} is the difference between the clear sky brightness temperature and the aerosol-contaminated brightness temperature, δT_{Sa} is the temperature difference between the surface and dust layers, $\bar{T}_{Sa}$ is the average of the temperatures of the surface and the dust layer, θ is the satellite zenith angle, B_λ is the black body spectral radiance at wavelength λ. $\bar{T}_B$ is the "observed" average brightness temperature of the surface and dust layer. The vertical distribution of aerosols has a significant impact on the atmospheric heating rate profile; aerosol dust changes the air temperature by absorbing and emitting infrared radiation. The vertical distribution of aerosols is related to the temperature of the aerosol layer, which then affects the infrared brightness temperatures. Also, the secant of the satellite zenith angle (θ) represents the increase in the optical path of the dust layer along an inclined propagation path, and consequences on the observed brightness temperature (Le Borgne et al. 2013).

Most of these studies addressed the effects of aerosol dust on the accuracy of the infrared satellite-derived SST_{skin} determined by comparisons with drifting buoy measurements, which have thermometers mounted typically 20 cm below the sea surface. However, the temperature variability between that depth and the surface contributes to the differences between the satellite-derived and buoy temperatures. The study reported here used remotely sensed SST_{skin} from the Marine-Atmosphere Emitted Radiance

Interferometers (M-AERI; Minnett et al. (2001)) mounted on research vessels to assess MODIS SST_{skin} under Saharan aerosol dust outflows, thereby removing the uncertainties introduced by temperature variability beneath the ocean-atmosphere interface.

This study focuses on the effects of aerosol dust on Terra MODIS-derived SST_{skin}, particularly the impact of the vertical distribution of the dust, and provides some suggestions for improving the accuracy of the SST_{skin} retrievals. In addition to the M-AERI SST_{skin} data, radiosonde air temperature and water vapor profiles collected from research cruises onboard the NOAA Ship *Ronald H. Brown (RHB)* and R/V *Alliance* were used. In Section 2, we introduce the MODIS TERRA SST_{skin} retrieval algorithms, the M-AERI and radiosonde measurements, the Modern-Era Retrospective Analysis for Research and Applications, Version 2 (MERRA-2; Gelaro et al. (2017)) dust profile data, Radiative Transfer for TOVS (RTTOV; Saunders et al. (2018)) model, and give an overview of the AERosols and Ocean Science Expeditions (AEROSE) ship-based field campaigns. Section 3 describes the in-situ match-up results. Section 4 provides a detailed quantitative analysis of the SST_{skin} differences through the use of radiative transfer simulations, including the effects of the temperature and height of the dust layer. Section 5 concludes the paper with a summary of our approach and findings.

2. Instruments and data

2.1 MODIS satellite data

The TERRA MODIS SST_{skin} retrievals from 2007 to 2019 are used in this study. Level 2 SST_{skin} data files were downloaded from https://disc.gsfc.nasa.gov/ . Each L2 SST_{skin} pixel contains a Quality Level (QL) indicator, with 0 indicating best quality and 4 the worst quality. We use in this study QL = 0, QL = 1 and QL = 2 data, the “best”, “acceptable”, and “suspect” quality data. QL = 0 and 1 data are preferred since they should be more accurate than those with QL = 2. As described in the MODIS SST_{skin} quality level flow chart (GSFC 2020), SST retrievals 3 K colder than a reference SST are assigned to QL = 2; however, the aerosol dust could introduce more than 3 K error in the retrieval, which is why QL = 2 data are included in this study. Also, there is a limit for situations where the impact of aerosols is so strong to produce situations similar to cloud cover.

The current MODIS SST_{skin} retrieval algorithm (GSFC 2020) is derived using a slightly modified nonlinear SST algorithm (NLSST; Walton et al. (1998)):

$$SST_{skin} = a_{ij0} + a_{ij1}BT_{11\mu m} + a_{ij2}(BT_{11\mu m} - BT_{12\mu m}) \times T_{sfc} + a_{ij3}(\sec(\theta) - 1) \times (BT_{11\mu m} - BT_{12\mu m}) + a_{ij4} \times M + a_{ij5}(\theta) + a_{ij6}(\theta)^2 \qquad \text{Equation (2)}$$

Where $BT_{11\mu m}$ and $BT_{12\mu m}$ are the top-of-atmosphere brightness temperatures derived from radiance measurements in the 11 and 12µm bands. M is the mirror side. T_{sfc} is the “first guess” SST based on SST4 4µm retrievals during nighttime and the Canadian Meteorological Center SST (Brasnett 2008) during daytime. T_{CMC} scales the brightness temperature difference correction due to water vapor column amount which is related to T_{sfc} (GSFC 2020; Walton et al. 1998). θ is satellite zenith angle. M is used to correct the potential differential degradation between the spectral reflectivity of the two mirror sides. a_{ij0} to a_{ij6} are the atmospheric correction coefficients derived with matched in-situ SST (Kilpatrick et al. 2015). Unlike the SLSTR on Sentinel-3a and -3b (Donlon et al. 2012; Merchant 2012) which have coefficients of the atmospheric correction algorithm derived through radiative-transfer modelling (Embury and Merchant 2012; Embury et al. 2012; Merchant 2012), the MODIS atmospheric correction coefficients are derived from regressions between MODIS brightness temperatures and collocated, coincident in-situ temperature measurements, and are set according to the month of year (*i*) and latitude bands (*j*).

The MODIS SST_{skin} atmospheric correction algorithm has been frequently updated, and the MODIS data have been reprocessed accordingly, so as to provide consistent high-quality fields by using improved atmospheric correction algorithms and cloud masks. The development of the MODIS NLSST algorithm is discussed by Brown and Minnett (1999), Kilpatrick et al. (2001), and Kilpatrick et al. (2015).

2.2 AEROSE cruises

All of the M-AERI and radiosonde data used here are from a series of AEROSE cruises (Morris et al. 2006; Nalli et al. 2011) in the tropical and subtropical Atlantic Ocean. Measurements taken during these cruises permit the quantification of the effects of Sahara dust aerosol on satellite retrievals and reanalysis fields. SST_{skin} is derived from M-AERI measurements. Radiosondes were launched from the ships every 4-8 hours depending on satellite overpass times. By using a total of 650 radiosondes from the AEROSE cruises, this study offers a valuable way to validate satellite SST_{skin} retrievals through atmospheres containing mineral dust and dry air layers originating from Africa; the dry layer effects on SST_{skin} retrievals from the measurements of MODIS on AQUA have been discussed by Szczodrak et al. (2014).

Table 1 summarizes the time, coverage, and the number of radiosondes deployed on the *RHB* and *Alliance*. Figure 1 shows the tracks of the ships; all of the plotted data points have valid M-AERI measurements which enable the study of the effects of the aerosol vertical distribution on the accuracies of the TERRA MODIS SST_{skin} products.

Table 1. Details of the AEROSE cruises used in this study.

CRUISES	NUMBER OF RADIOSONDES	START	END	DAYS OF DATA
2007 RHB	96	2007-05-07	2007-05-28	22
2008 RHB	74	2008-04-29	2008-05-19	21
2009 RHB	78	2009-07-11	2009-08-11	31
2011 RHB	102	2011-07-21	2011-08-20	31
2013 RHB	111	2013-11-11	2013-12-08	28
2015 Alliance	92	2015-11-17	2015-12-14	28
2019 RHB	97	2019-02-24	2019-03-29	34
Total	**650**	**2007-05-07**	**2019-03-29**	**195**

RHB: NOAA Ship *Ronald H. Brown.*
Alliance: North Atlantic Treaty Organization (NATO) R/V Alliance.

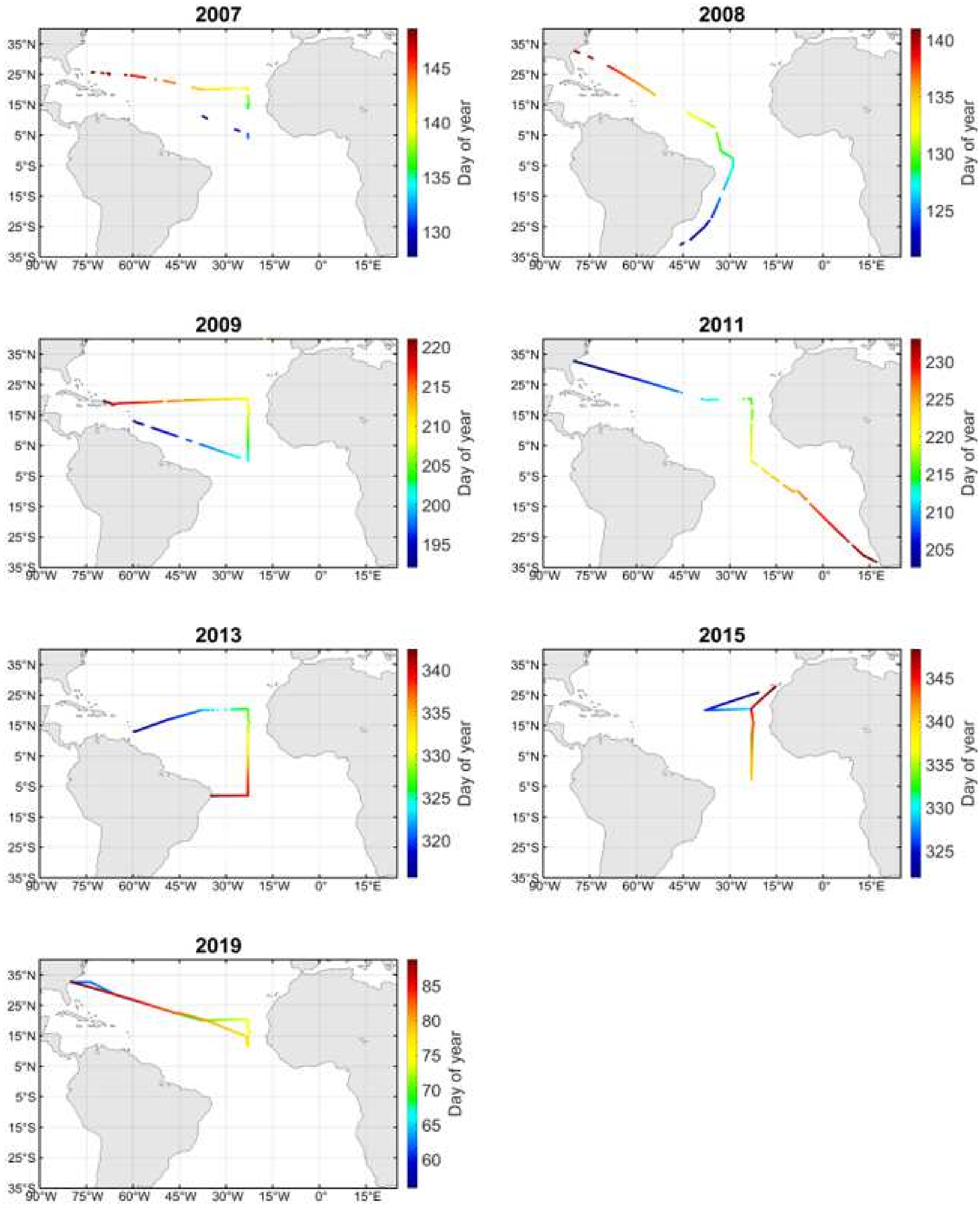

Figure 1. Cruise tracks of each AEROSE campaign. The colors indicate the day of year. Gaps indicate where M-AERI measurements were not made due to the instrument entering safe mode during rain or sea-spray events, or instrument repairs.

2.2.1 M-AERI

M-AERIs are hyperspectral interferometric Fourier Transform Infrared (FTIR) radiometers that measure the infrared emission spectra of the ocean surface and atmosphere from which SST_{skin} can be derived (Minnett et al. 2001). These are directly comparable to the MODIS SST_{skin} retrievals. M-AERIs are mounted a few meters above the sea surface on the ships, as shown in Figure 2 (bottom).

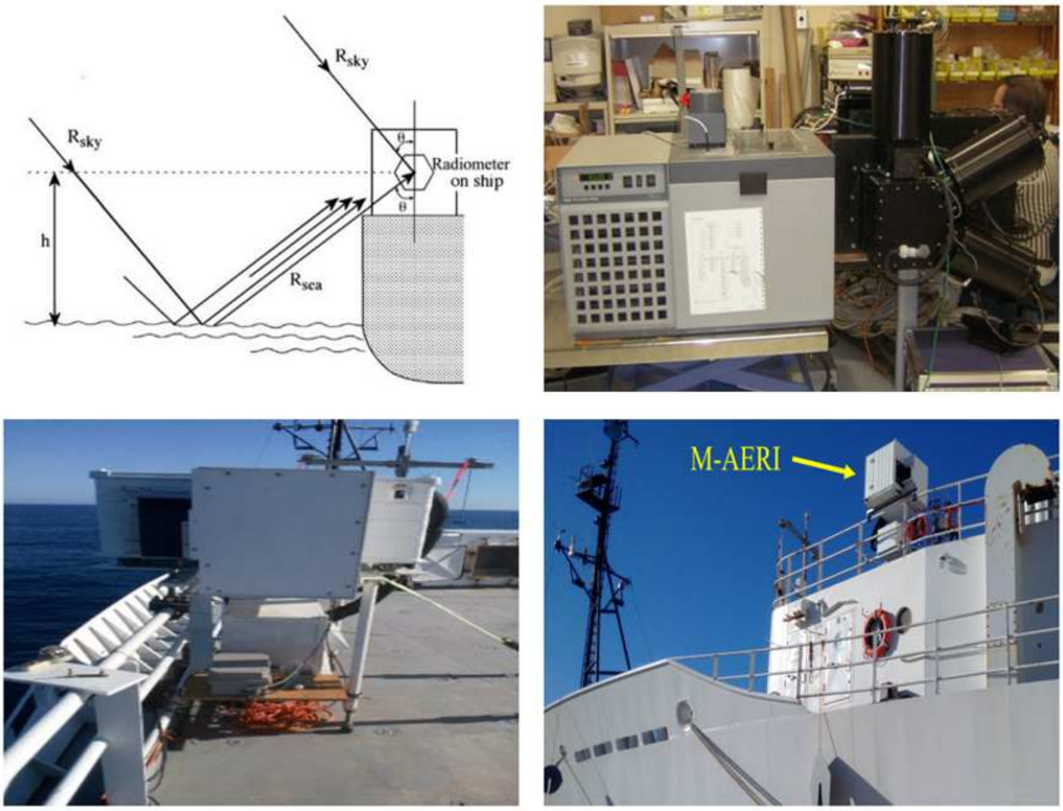

Figure 2. Top left: Viewing geometry of M-AERI. Top right: The M-AERI internal calibration is checked in the laboratory before and after each deployment using an external calibration procedure. Bottom: Installations of M-AERI on the NOAA ship Ronald H Brown (RHB). The M-AERIs are inside hermetically sealed aluminum enclosures with only the scan mirror and calibration black-bodied being exposed to the open air, but protected. The smaller boxes beneath contain air-conditioning units that limit temperature and humidity variations in the instrument enclosures.

Figure 2 (top left) shows the viewing geometry of M-AERI; two internal blackbodies provide a two-point calibration before and after each measurement of the sea-surface and sky infrared emission spectra. The sky radiance reflected from the sea surface is corrected using the sky emission measurements as described by Minnett et al. (2001). The M-AERI SST_{skin} is derived from measurements at a wavelength of 7.7 µm to reduce the sensitivity to atmospheric variability (Smith et al. 1996). Figure 2 (top right) shows the M-AERI calibration being checked in our laboratory, which happens before and after each deployment, by measuring the emission from a water-bath calibration target of National Institute of Standards and Technology (NIST) design (Fowler 1995) which has calibration traceability to standards at NIST (Rice et al. 2004) and at the UK National Physical Laboratory (Theocharous et al. 2019). The M-AERI data are extremely useful to provide measurements for validating and improving satellite-derived variables (Luo et al. 2019; Szczodrak et al. 2014) and reanalysis products (Luo and Minnett 2020; Luo et al. 2020b) under various situations.

2.2.2 Radiosondes

Vaisala RS92 radiosondes were launched during the AEROSE campaigns to measure atmospheric values of temperature and humidity. Radiosondes take measurements every second from the surface to typically 100 hPa, which results in a very high vertical resolution (~0.1 hPa) depending on the speed of ascent. Radiosonde data provide input for the radiative transfer model to simulate the MODIS measurements under various aerosol dust loads, derived from the MERRA-2 fields, to assess the degradation of the accuracies of the MODIS SST_{skin} retrievals. The radiosonde data indicate the presence of anomalies in the atmospheric profiles, such as dry layers or the near-surface warm dust layer. Atmospheric relative humidity and air temperature sections from radiosondes along the cruise tracks (Figure 1) are presented in Figures 3 and 4. The x-axes are the day of the year.

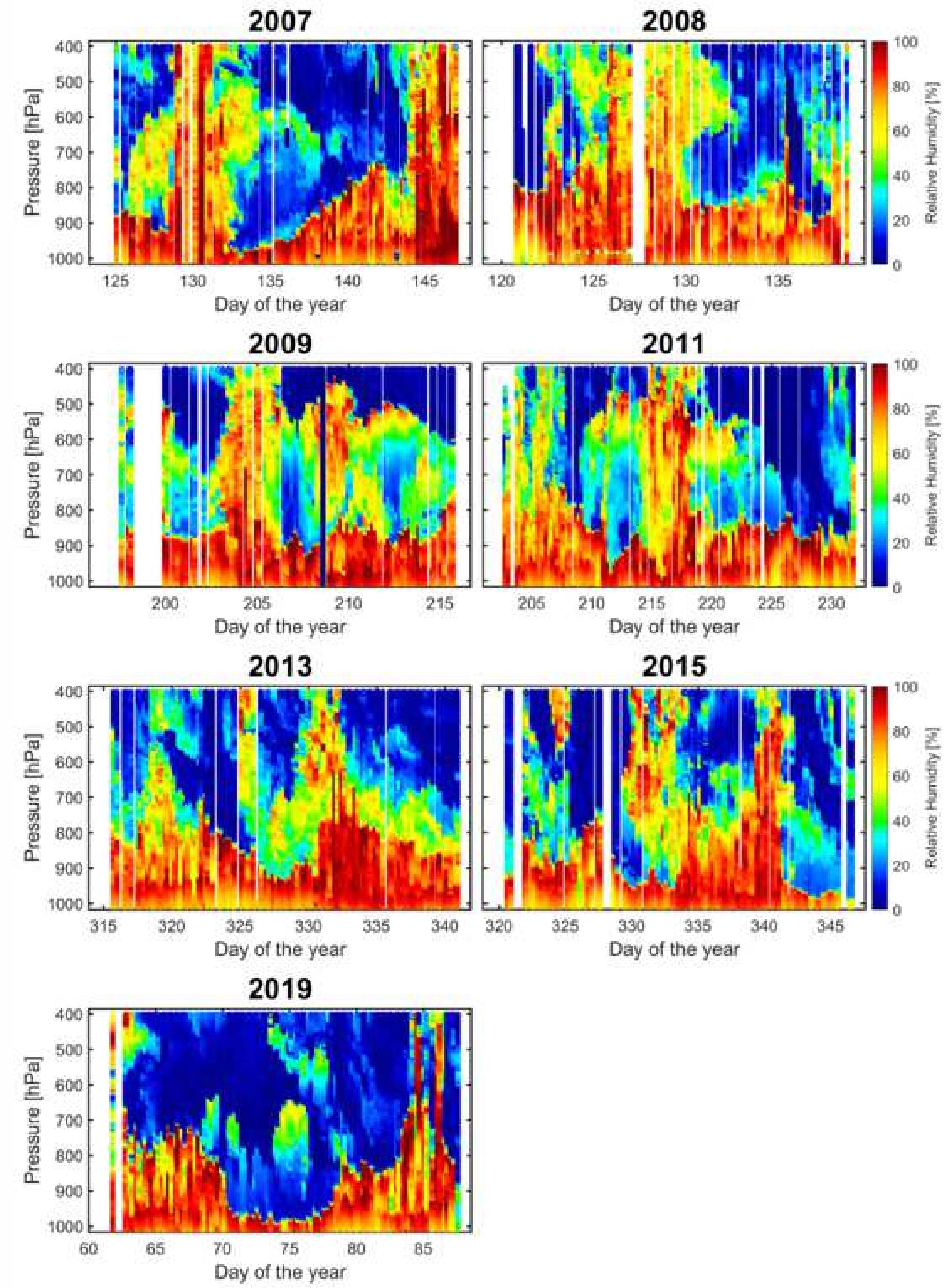

Figure 3. Relative humidity measured by radiosondes launched from the ships. Colors indicate the relative humidity. The dust dry layers are clearly visible on days 135-142 of

2007, 127-131 of 2008, 205-210 of 2009, 210-215 of 2011, 325-333 and 341-347 of 2015, and 68-79 of 2019, usually from the surface to 700 hPa.

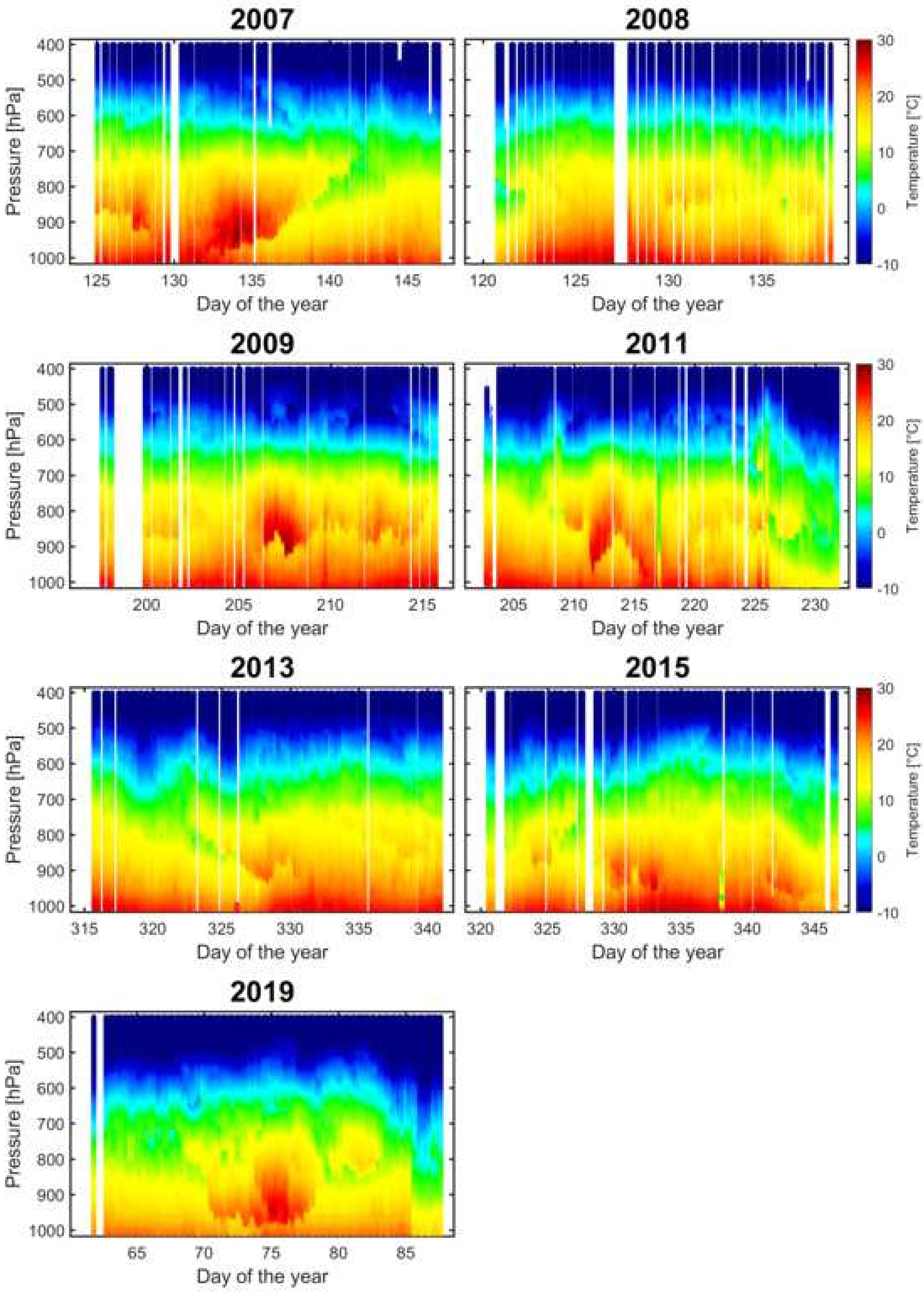

Figure 4. As Figure 3, but for air temperature. The color indicates temperature according to the scale at right. The unit is ^{o}C.

2.3 MERRA-2

The MERRA-2 reanalysis model output was generated in NASA's Global Modeling and Assimilation Office Data Assimilation System (Bosilovich et al. 2015; Gelaro et al. 2017) and is available through http://disc.sci.gsfc.nasa.gov/mdisc/. MERRA-2 fields are calculated on a regular geographic grid at a spatial resolution of approximately 0.625° × 0.5° in longitude × latitude. The MERRA-2 data contain geolocated, derived geophysical variables, including aerosol dust mixing ratio used in this study, at 72 standard pressure levels. MERRA-2 assimilates the dust profile from various ground-based as well as space-based sources; details of the MERRA-2 dust profile assimilation is described by Randles et al. (2017). MERRA-2 has five size bins for dust aerosols spanning 0.1 µm to 10 µm radius, from which the subsets of bin 2 (1 µm to 1.5 µm) and bin 3 (from 1.5 µm to 3 µm) were used in this study, since they are more widely spatially distributed (Haywood et al. 2005) and have a strong effect on IR radiative transfer.

We use dust mixing ratio values from MERRA-2 to conclude the effects of the vertical aerosol dust outbreaks on MODIS derived SST_{skin}. Figure 5 shows the corresponding MERRA-2 value. The MERRA-2 dust values used in this study have a 3-hour temporal resolution (Buchard et al. 2017; McCarty et al. 2016; Randles et al. 2017); MERRA-2 aerosol values were linearly interpolated in time and bi-linearly interpolated in space to the ship positions and times.

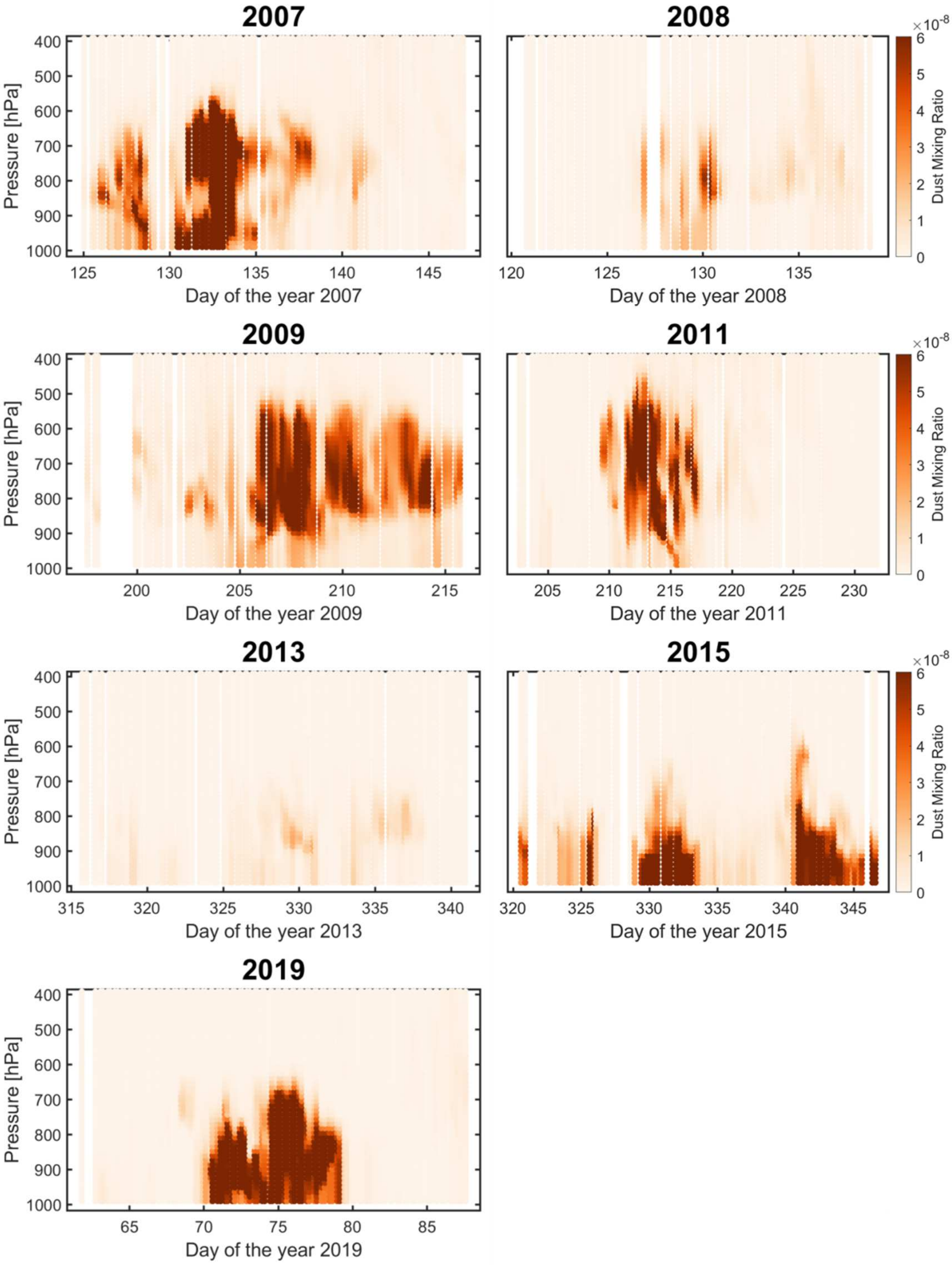

Figure 5. MERRA-2 dust mixing ratio sections of each AEROSE track, only the days with valid radiosonde data are plotted. Color indicates dust mixing ratio as shown on the

right. White vertical lines indicate where radiosondes were not deployed due to inclement weather or other reasons. The dust mixing ratio is kg/kg.

2.4 RTTOV

RTTOV is a fast radiative transfer model developed by the UK Met Office and Météo-France within the Numerical Weather Prediction Satellite Application Facility (NWP-SAF) (Saunders et al. 2018). RTTOV simulates measurements of radiometers on satellites, and is widely used by satellite remote sensing communities. Simulations of brightness temperatures have many applications, such as improving MODIS SST_{skin} retrievals under aerosol dust conditions (Luo et al. 2019), and developing cloud mask for operational SST retrieval (Merchant et al. 2005), etc. Air temperature and relative humidity at pressure levels through the atmosphere, SST_{skin}, and other inputs are needed to perform brightness temperature calculations. Measurements from radiosondes and M-AERIs, and the aerosol information from MERRA-2, described above, provide the atmospheric and surface parameters for the brightness temperature calculation. RTTOV version 12.3, used here, is available from https://www.nwpsaf.eu/site-/software/rttov/.

3. SST_{skin} Assessment

This study investigated the aerosol dust effects on the SST_{skin} retrievals from MODIS against the well-calibrated M-AERI SST_{skin} values in the Atlantic Ocean. It is necessary to note that this study only examines the TERRA MODIS SST_{skin} data with a QL < 3 and pixels that have been confidently identified as being cloud contaminated are not used.

A Match-Up Data Base (MUDB) was generated to compare the MODIS SST_{skin} fields with M-AERI SST_{skin} retrievals. 'match-up' stands for a data vector that consists of MODIS derived SST_{skin}, M-AERI SST_{skin}, MERRA-2 dust concentrations, and other relevant parameters. Match-ups are co-located between satellites and M-AERI data taken within 30 minutes and 10 km of latitude and longitude (Donlon et al. 2014a; Kilpatrick et al. 2015). Additional variables are included in each MUDB record, including the MODIS infrared brightness temperatures and parameters of the satellite instrument viewing geometry.

All of the AEROSE cruises included regions of Saharan dust outflow. The dust can be lifted up to 500 hPa and transported over the North Atlantic Ocean as shown in Figure 5. The dust mixing ratio distributions from MERRA-2 along the ship tracks indicate large scale Saharan dust outflow on days 135-142 of 2007, 127-131 of 2008, 205-210 of 2009, 210-215 of 2011, 325-333 and 341-347 of 2015, and 68-79 of 2019. Figures 3 and 4 show that the elevated dust layers are sometimes associated with dry air layers; the dry layer effect on MODIS derived SST_{skin} has been discussed by Szczodrak et al. (2014) who found that anomalous dry layers can introduce both positive and negative errors in MODIS SST_{skin} retrievals dependent on the height of dry layers. However, there were some days when the dry layers were not associated with dust layers, such as the days 135-140 of 2008 and the days 220-232 of 2011; also there were some days the dust was in moist layers such as the days 130-132 of 2007 and the days 214-216 of 2011. The dust may absorb the shortwave radiation and warm the lower tropospheric temperature (Choobari et al. 2014; Twomey 1972), also as shown in the radiosonde measured air temperature (Figure 4). The air temperature and relative humidity anomalies associated with aerosol dust layers were captured by the radiosonde data used in this research. Therefore, the AEROSE cruises provide an opportunity to test the accuracies of the MODIS SST_{skin} values under a variety of meteorological conditions.

This study is limited to conditions in which the cloud screening algorithms indicate cloud-free skies as the match-up pairs have been subjected to the updated cloud mask (Kilpatrick et al., 2019b). The SST_{skin} differences are defined as MODIS minus M-AERI. To illustrate the aerosol dust effects, Figure 6 shows the SST_{skin} differences and MERRA-2 dust mixing ratios (Figure 5), as a function of time along the ships' tracks, according to the color bar at the right side.

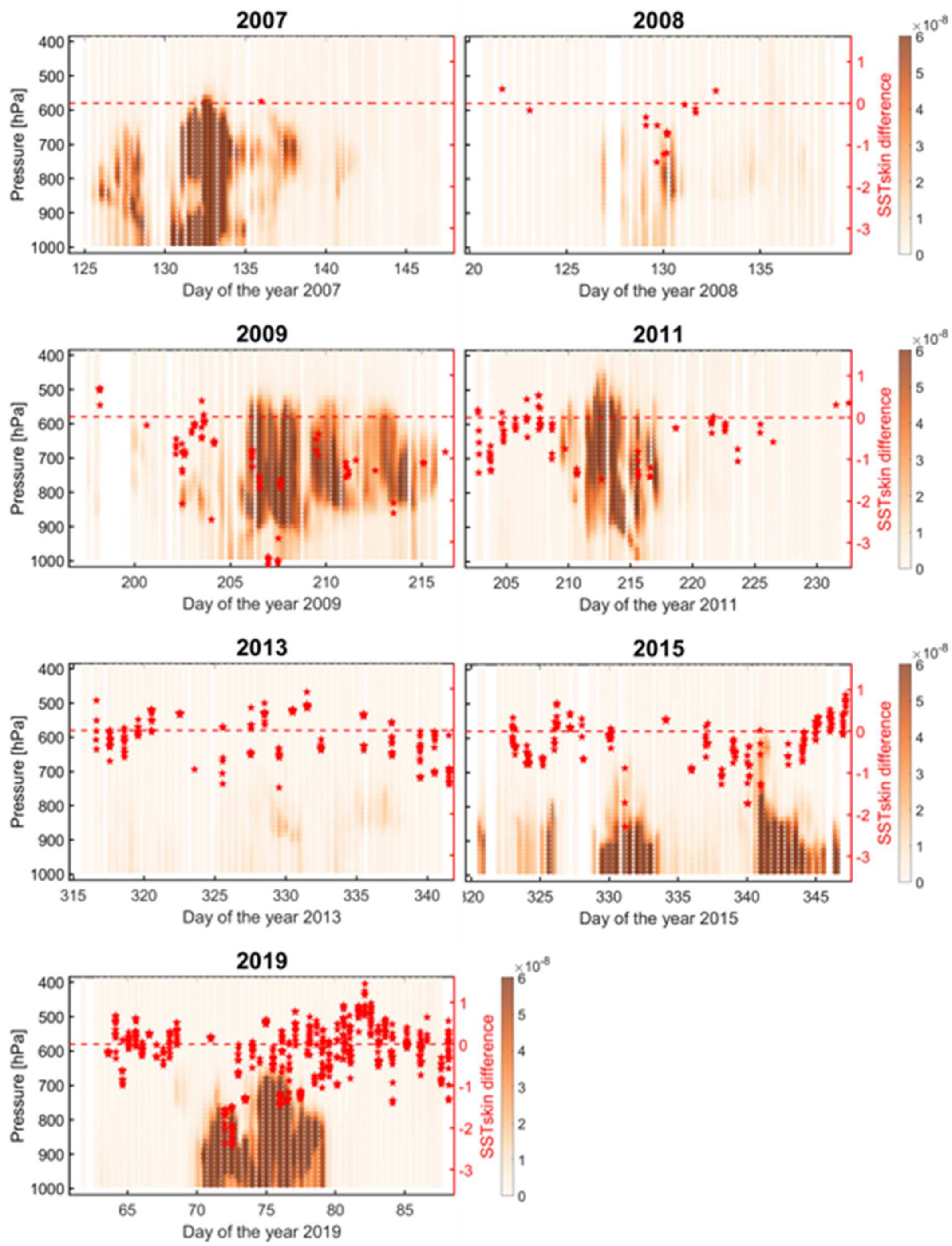

Figure 6. SST_{skin} difference from each of the ship tracks. Red stars indicate the difference with the right y-axis range. The operations of M-AERIs are suspended during rain thus

causing some SST_{skin} data gaps along the track. Comparisons in and close to ports are not used. The background color indicates the MERRA-2 dust mixing ratio.

Although the AEROSE 2008 cruise has relatively few match-up points, the available pairs around days 127-131 show colder MODIS SST_{skin} temperatures when dust is present (Figure 6), and although the dust concentration is quite small, it occurs at high-altitude and its relatively cold temperature (12°C – 14°C for dust layers and 27°C – 30°C for SST_{skin}) leads to a comparable MODIS SST_{skin} retrieval error to situations where denser dust layers occur lower in the atmosphere, such as in 2015 and 2019, There are strong Saharan dust outbreaks along the AEROSE 2009 tracks across the Atlantic Ocean (Figure 1). The SST_{skin} difference is positive at the beginning of the 2009 cruise in the absence of dense dust, but being in the range of minus 1 K to 0 K for days 202-204 when the dust concentration was moderate. On the days when the *Ronald H. Brown* entered significant, large-scale Saharan dust outflow events, the negative SST_{skin} differences were more pronounced: the averaged SST_{skin} difference being as large as -3 K between days 205-210. AEROSE 2011 also encountered a strong dust outbreak, with the averaged SST_{skin} difference being ~ 1K for days 210-216. The dust-layer temperature was high (22°C – 28°C for dust layers and 23°C – 26°C for SST_{skin}) during days 211-214 of 2011, as shown in Figure 4, indicating a dry, warm dust layer which resulted in negative MODIS SST_{skin} retrieval errors, but which are not as large as during AEROSE 2009. A strong dust outbreak was not encountered during AEROSE 2013. Depending on other factors, such as the characteristics of the dry layer, the SST_{skin} difference may be positive or negative (Szczodrak et al. 2014). The 2015 AEROSE cruise was onboard the R/V *Alliance*, and began on November 15 in Las Palmas, Gran Canaria, and ended on

December 14 in the same port, as shown in Figure 1. The Saharan dust outbreaks were encountered many times during AEROSE 2015 (Figure 6), thus providing several sets of measurements of the effects of dust outflow over the Atlantic Ocean. When the R/V *Alliance* first entered a significant and large-scale Saharan dust outflow on days 323-326 of 2015, the dust layer extended in the vertical to ~850 hPa and the corresponding SST_{skin} differences were in the range of ±1 K. For the second Saharan dust encounter, on days 328-333, the SST_{skin} differences are negative, up to -2.5 K, with a dust layer with an extensive vertical extent and high concentration. It is interesting to note that at the third dust encounter from days 339-347, the SST_{skin} difference gradually changed from negative to positive, possibly due to the dust layer altitude, humidity and temperature: there were dry and warm anomalies at 850-1000 hPa, the positive SST_{skin} differences during day 346 appear to have been caused by an anomalous warm temperature of the dust layer near the port of Las Palmas, Gran Canaria. AEROSE 2019 began and ended in Charleston, South Carolina. Most of the days during this cruise were under clear-sky conditions; therefore, there are more match-up pairs between MODIS and M-AERI than in other years. The MERRA-2 fields and radiosonde values clearly indicate the presence of the warm and dry dust layer in days 70-77 (Figures 3 and 4). The results show a pronounced SST_{skin} difference, sometimes more than -3 K, linked to the dust layer. The overall SST_{skin} difference is negative, however, when the upper-tropospheric dust layer is extremely warm and humid, as on day 75, the SST_{skin} difference is positive, ~0.8 K.

Equation (1) describes the theoretical sensitivity of top-of-atmosphere brightness temperatures to an aerosol dust layer. The dust cooling effect can cause the temperature difference between the surface and dust layers δT_{sa} to become negative, thus the corresponding infrared brightness temperature, such as $BT_{11\mu m}$ and $BT_{12\mu m}$ in Equation (2), will decrease.

Combining Equation (1) and Equation (2), for the satellite zenith angle at nadir, and ignoring the small mirror-side term, the Terra MODIS SST_{skin} difference due to the $BT_{11\mu m}$ and $BT_{12\mu m}$ changes can be expressed as

$$\Delta SST_{skin} \approx b_{ij0} + [1 - \exp(-\tau_{\lambda a})] \times \delta T_{sa} \times \{b_{ij1} \frac{\left(\frac{\partial B_{\lambda 11\mu m}}{\partial T}\right)_{\bar{T}_{Sa}}}{\left(\frac{\partial B_{\lambda 11\mu m}}{\partial T}\right)_{\bar{T}_B}} + b_{ij2} \times T_{sfc} \left[\frac{\left(\frac{\partial B_{\lambda 11\mu m}}{\partial T}\right)_{\bar{T}_{Sa}}}{\left(\frac{\partial B_{\lambda 11\mu m}}{\partial T}\right)_{\bar{T}_B}} - \frac{\left(\frac{\partial B_{\lambda 12\mu m}}{\partial T}\right)_{\bar{T}_{Sa}}}{\left(\frac{\partial B_{\lambda 12\mu m}}{\partial T}\right)_{\bar{T}_B}} \right] \}$$

Equation (3)

b_{ij0} to b_{ij2} are the similar atmospheric correction coefficients as a_{ij0} to a_{ij6} in Equation (2). As shown in Equation (3), the SST_{skin} retrieval difference (ΔSST_{skin}) depends on the aerosol dust optical depth τ_{va} and the temperature difference between the surface and dust layers δT_{Sa}, the results presented here are consistent with this simple expression.

Thus, expecting the SST_{skin} bias should be increased with the dust layer concentration and temperature difference with respect to the SST_{skin}, we define the following SST_{skin} bias factor ($\Delta SST_{aer\_\delta T}$) as

$$\Delta SST_{aer\_\delta T} = \sum_{p=surface}^{p=400hPa} \sum_{i=3}^{i=1} (SST_{skin} - T_{air}) \times x_i \times \beta_{ext,i}$$

Equation (4)

Where x_i is each layer's MERRA-2 dust mixing ratio of bins 1, 2 and 3 with the effective dust radii of 0.64, 1.34 and 2.32 mm, respectively, $\beta_{ext,i}$ is the sum of scattering and absorption coefficients, as mass extinction coefficient of each dust bin, their values are taken from supplementary tables of Randles et al. (2017). T_{air} is the air temperature of the corresponding layer, SST_{skin} is the M-AERI measured skin temperature. The $\Delta SST_{aer\_\delta T}$ is integrated from the sea surface up to 400 hPa. Figure 7 shows the relationship between $\Delta SST_{aer\_\delta T}$ and the MODIS SST_{skin} retrieval bias. Only the match-up pairs with MERRA-2 total AOD > 0.05 are included in Figure 7. There is an overall negative correlation between them, when the $\Delta SST_{aer\_\delta T}$ > 1.5×10^{-5}, the averaged difference is > 1 K.

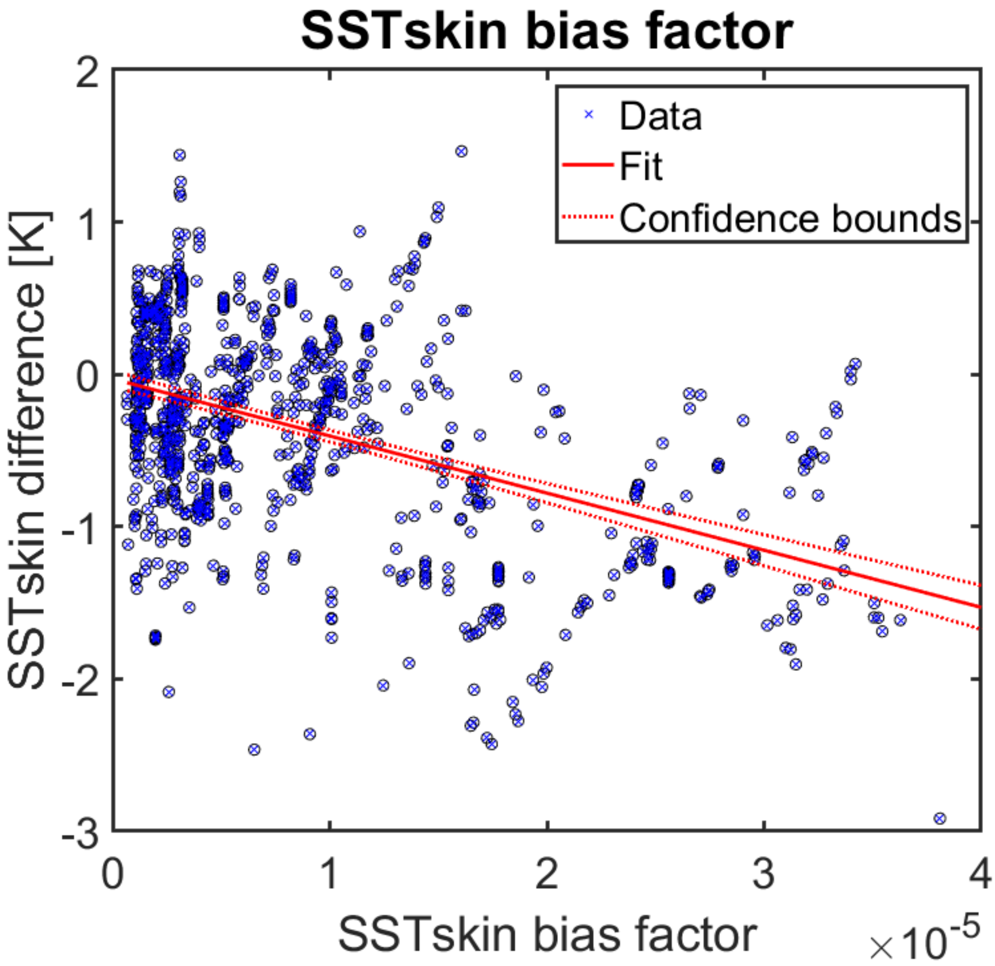

Figure 7. The relationship between MODIS SST_{skin} retrieval bias and $\Delta SST_{aer\_\delta T}$. The red line is the fitted linear regression line.

As indicated by Brown and Minnett (1999), Merchant et al. (2006), Good et al. (2012), and Luo et al. (2019), the aerosol dust causes the split-window difference of $(BT_{11\mu m} - BT_{12\mu m})$ to decrease due to the spectral character of dust absorption in the long wavelength infrared window, thereby confounding the correction of the clear-sky atmospheric effect, due primarily to water vapor, in the SST_{skin} retrieval. Overall, the dust particles in the higher atmosphere introduce more negative errors into the retrieved SST_{skin}.

By using the AEROSE MUDB, this study revealed the impacts of the dust layer vertical distribution on the MODIS-derived SST_{skin}. The comparison shows that the infrared satellite-derived SST_{skin} negative differences are mainly localized in the Saharan dust outflow region. The SST_{skin} retrieval error is related to the concentrations, altitudes, and temperatures of dust layers.

4. RTTOV Simulation Assessment and Discussion

Inaccuracies in the TERRA MODIS retrieved SST_{skin} can be investigated by using atmospheric radiative-transfer modeling. Brightness temperature simulations for TERRA MODIS infrared channels 31 ($\lambda = 11$ μm) and 32 ($\lambda = 12$ μm) have been performed with the RTTOV model, and the brightness temperatures are used to derive SST_{skin} according to Equation 2. The internal RTTOV climatological type was held constant as "7: Maritime polluted" to let the dust aerosol load over the ocean throughout the simulations. The aerosol particle type was set as "Mineral Transported" from the Optical Properties of Aerosols and Clouds index (OPAC; Hess et al. (1998))" . The RTTOV model was run with radiosonde measured air temperature and humidity profiles and MERRA-2 dust concentrations in Section 4.1, and with fixed atmospheric temperature and humidity but with variable dust profiles in Section 4.2. In section 4.1, the MERRA-2 dust mixing radio was directly loaded into RTTOV for each pressure layer with the aerosol concentration unit set as "kg/kg". In section 4.2, simulations were conducted with varying dust concentrations set at different vertical layers in the atmosphere. The solar and satellite zenith angles are set to 0 in all the simulations to avoid the complications of slant path attenuation as discussed by Nalli et al. (2012). The aerosol dust-induced SST_{skin} error described in this section is defined as the dust aerosol-contaminated SST_{skin} retrieval minus the “without dust” derived SST_{skin}, with a negative value indicating an error to colder SST_{skin} retrievals due to the dust aerosol.

4.1 Radiative Transfer Simulations

Since the occurrence of the dust layer is often accompanied by clouds, such SST_{skin} retrievals have been flagged as poor quality, for example, there are few match-up pairs from the AEROSE 2007 cruise. However, we can use RTTOV to simulate the dust effect on TERRA MODIS-derived SST_{skin}.

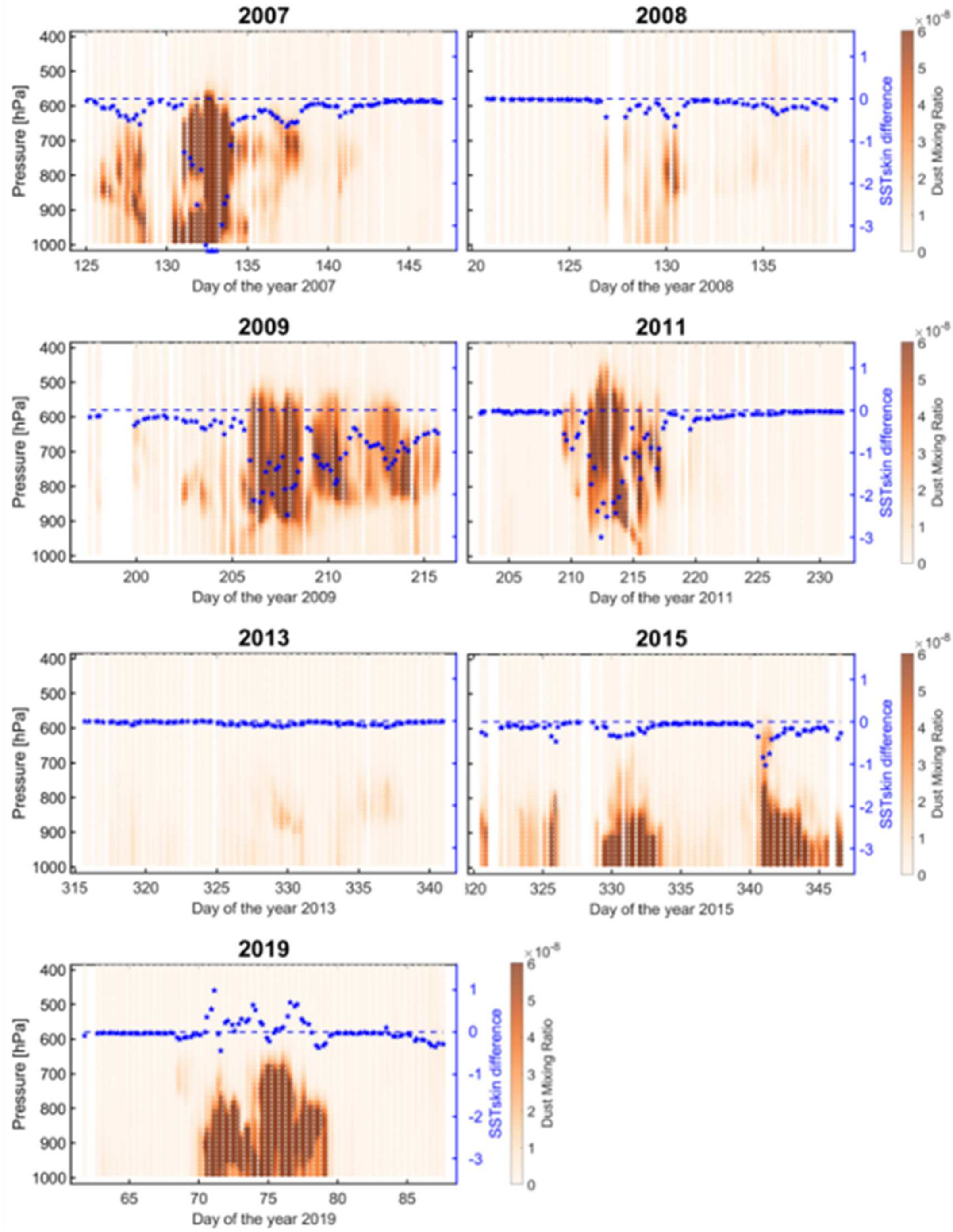

Figure 8. SST_{skin} differences from RTTOV simulations along the cruise tracks. The blue stars indicate the simulated SST_{skin} error caused by the aerosol according to the y-axis scale at right. The background color indicates the MERRA-2 dust mixing ratio.

Input for the aerosol-free RTTOV simulations are SST_{skin} from M-AERI, and air temperature and humidity from radiosondes. We ran the RTTOV without dust aerosol to simulate the TERRA MODIS clear-sky brightness temperature measurements, then deriving the SST_{skin} using the standard MODIS NLSST atmospheric correction algorithm (Equation 2). Dust mixing ratios from MERRA-2 are used to give the locations and concentrations of the aerosol dust. The derivation of SST_{skin} was repeated with simulations including the MERRA-2 dust values. The difference between the retrievals reveals the SST_{skin} retrieval error under dust aerosol influence. Figure 8 shows the RTTOV simulated results along each AEROSE cruise in this region; the blue stars are the simulated SST_{skin} error associated with the right y-axis. The left y-axis indicates the RTTOV pressure layer.

The results from AEROSE 2007 to 2011 show that the negative SST_{skin} difference can be marked when the ship entered significant, large-scale Saharan dust outflow regions. Moreover, the uncertainties are related to the dust layer thickness and altitude. The intense dust outbreaks during days 132-133 of 2007, days 206-209 of 2009, and days 212-213 of 2011 can introduce simulated differences of -3 K to -4 K. AEROSE 2013 did not encounter significant dust outbreaks; the low concentration dust layers during days 326-332 sill introduced some SST_{skin} error, but within 0.05 K. The AEROSE 2015 passed through a few Saharan dust outbreak regions, which can be seen in the background MERRA-2 dust mixing ratio values. For days 340-342 of 2015, the thick dust layer, extending from the surface to ~600 hPa introduced up to -1 K negative SST_{skin} retrieval errors. The -1 K error is smaller than for 2007, 2009, and 2011, because the dust layer was below 850 hPa for these days in 2015, so the dust layers were not lifted to higher altitudes as in 2007, 2009 and 2011. The SST_{skin} difference is related to the dust layer temperature; for a layer in the upper troposphere, it was found that both warming and cooling effects can be introduced by dust. On the other hand, when the dust layer appears in the lower troposphere, the warming effects dominate. The Saharan dust radiative heating rates to the air temperature vary with the situation (Carlson and Benjamin 1980); the maximum dust temperatures are usually near the maximum dust concentration level and near the surface. The negative errors from days 343 to 347 of 2015 were thus weakened because of the warm temperature of the dust layer. The AEROSE 2019 results illustrate the warm dust layer effects on the simulated SST_{skin}: some of the simulated errors are positive, up to 1K, for days 71-77. The results from in-situ validation (Section 3) and RTTOV simulations (Section 4.1) were reasonably consistent with each other, indicating it is necessary to know the dust loading altitude and temperature to assess their effects on satellite-derived SST_{skin}.

4.2 McClatchey Standard Profile simulation

Although the in-situ match-up measurements and RTTOV simulations demonstrate a clear trend of an increasing error with denser and higher dust layers, the SST_{skin} retrieval sensitivity to varying vertical distributions can be better determined by simulations with a fixed atmospheric profile. Determining the sensitivity is the subject of this section. The RTTOV model was run with fixed atmospheric conditions taken from the McClatchey Standard Tropical Profile (McClatchey 1972), together with various dust concentrations and vertical distributions. The fixed standard atmospheric profile makes it possible to assess the impacts of the dust layer heights and dust layer temperature as all other variables are held constant. Saharan dust outbreaks can be found at any height from the surface up to 6 km, often depending on their transport ranges, sources and other environmental variables such as wind, air temperature, etc. (Karyampudi et al. 1999). Dust is inserted at four different altitudes in this study, corresponding to the defined RTTOV pressure levels shown in Table 2. The dust concentration is varied from 0 to 1000 particles per cm^{-3}, in increments of 10.

Table 2. Dust layer altitude range, corresponding RTTOV pressure layers and the mean air temperature of this layer.

Altitude	Pressure	Mean air temperature
0 km – 1 km	922 hPa, 957 hPa, 985 hPa, 1005 hPa	297K
1 km – 2 km	795 hPa, 839 hPa, 882 hPa	291K
2 km – 3 km	702 hPa, 749 hPa	286K
3 km – 4 km	610 hPa, 656 hPa	280.5K

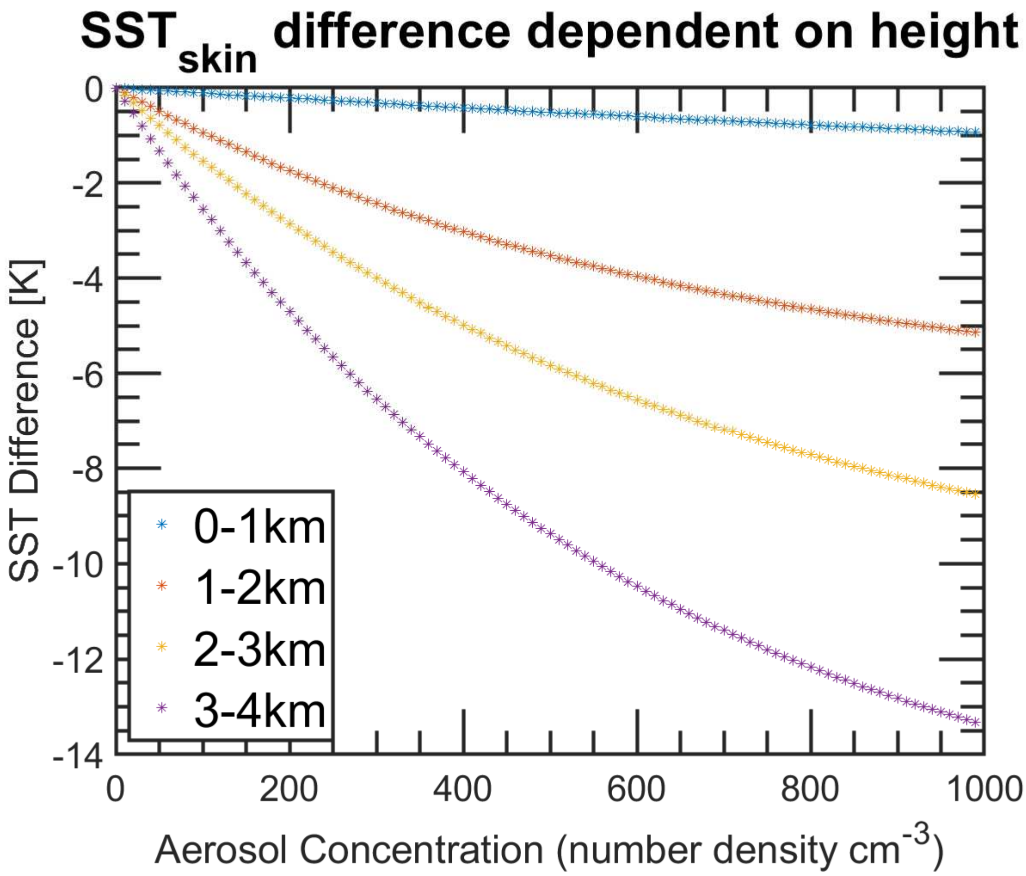

Figure 9. RTTOV simulation results showing the impact on the SST_{skin} retrieval of the altitude of the aerosol layer. Different colors indicate different altitudes of the dust layer. As the aerosol height is increased, the SST difference becomes more negative, except for very small concentrations.

The SST_{skin} error introduced by dust aerosol is shown in Figure 9, with different colors indicating different altitude ranges into which the dust was inserted. All of the simulations show a cooling effect due to dust; as expected, the cooling varies over a range of aerosol concentrations and dust heights. As shown in Figure 9, dust present at lower altitudes introduces a smaller SST_{skin} error as the temperature contrast with the sea surface is smallest. The only two variables in Figure 9 are difference in the simulated SST_{skin} retrievals with and without dust aerosols, and dust aerosol concentrations.

To further investigate the physical mechanism of the aerosol effect on satellite-derived SST_{skin}, this study explores the aerosol warming and cooling. Adebiyi et al. (2015) highlight the differences in the vertical temperature structure associated with different AODs. The temperature of the boundary layer top is up to 2 K colder when aerosols are present. The composite profile from polluted days (AOD > 0.2) reveals a previously documented warmer temperature anomaly at a lower atmospheric layer around 1000 hPa, capped by a colder anomaly at 600 hPa. Weaver et al. (2002) calculated the radiative forcing of Saharan aerosol dust, finding an increase of TOA longwave radiation with aerosol loading and observing that the aerosol dust absorbs infrared radiation and emits at a lower temperature. Hansell et al. (2010) and Wong et al. (2009) also identified the same vertical radiative effect of the Saharan dust layer: strong positive heating rates occur in the lowest layers and the heating rates are negative in the upper troposphere.

As discussed above, the Saharan aerosol dust can introduce air temperature anomalies according to their sources, altitude, or spatial distributions. The RTTOV model simulations included modifications to atmospheric temperatures covering a range of values that might result from the effects of the dust layers to determine their effects on satellite-retrieved SST_{skin}. Figure 10 shows the results after adding positive or negative temperature anomalies at different heights, indicated by the y-axis, with 0.1 K increments. The input SSTskin was set to 298 K. This simulation study has used step functions of adding the temperature anomalies to the aerosol layer. Evidence of dry layers in data from radiosonde profile generality show a very sharp temperature and humidity changes at both the lower and upper boundaries. To avoid statically unstable atmospheric situations, the temperature anomalies are limited as -5K to 5K.

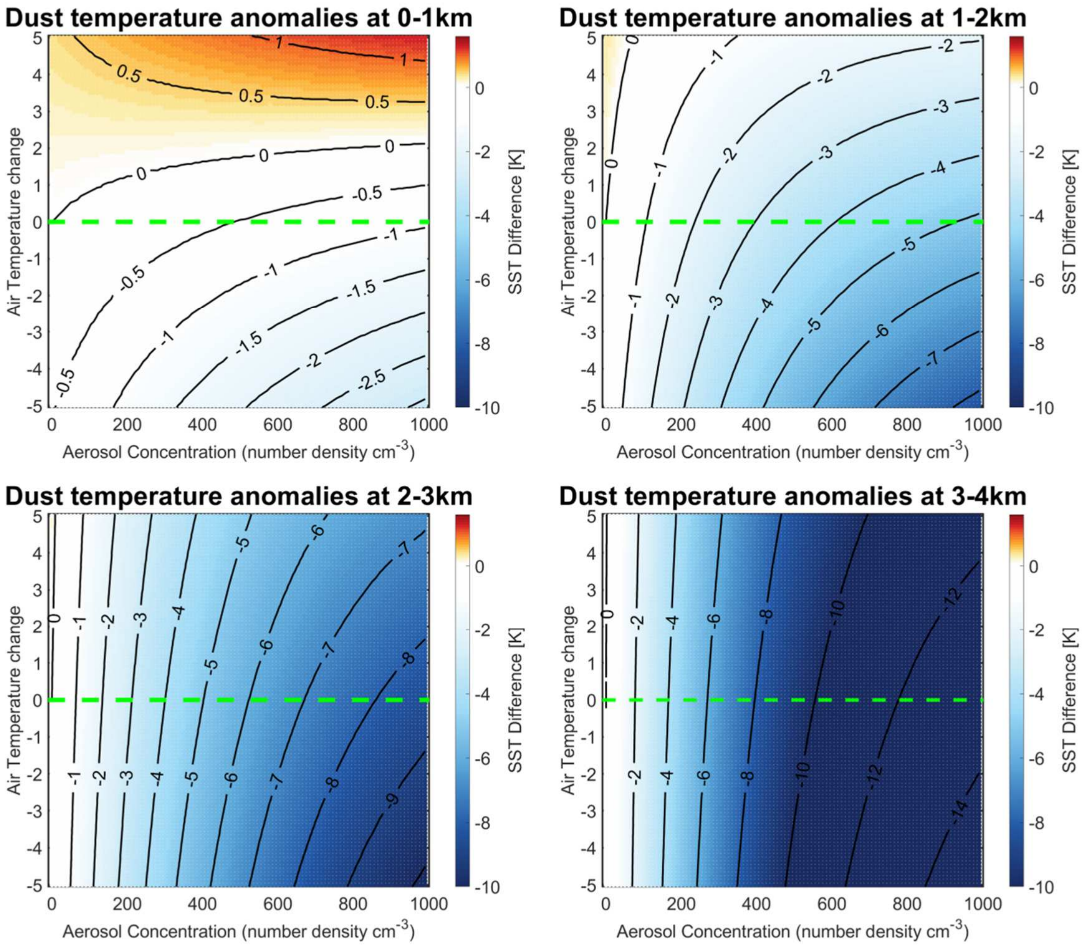

Figure 10. The effects on the SST_{skin} retrievals of the presence of air temperature anomalies of different magnitudes at various heights. The color indicates the SST_{skin} difference resulting from temperature changes in the aerosol layers. The x-axis is the aerosol concentrations at different heights as shown in the title. The y-axis is the aerosol layer temperature anomalies. The lines at y = zero emphasize the change in sign of the air temperature anomalies. The results show that the SST_{skin} difference is related to the dust layer temperature change, dust concentrations and altitude.

The parts above the green lines in Figure 10 illustrate the aerosol loading conditions with warmer temperature anomalies in lower atmospheric layers. The thick and warm dust layer load in the height range of 0-1 km can introduce differences in derived SST_{skin} of up to 1.5 K; and the warm dust at heights of 1-2 km can also deliver positive SST_{skin} retrieval differences. These results are comparable to those found in Section 3 with in-situ measurements and MERRA-2 dust concentrations, such as towards the end of AEROSE 2015 cruise under the Saharan dust, the dense and warm dust layer near Las Palmas introduced a positive SST_{skin} error. The parts below the green lines in Figure 10 show that the high-altitude dust over the tropical ocean contributes considerably to the strong negative errors in those simulations.

As expected, introducing the cold temperature anomalies to the dust layer the overall aerosol dust cooling effects are stronger in each simulation for the dust at various altitudes. The bottom panels with dust present at 2-3 km and 3-4 km show a sharp increase of negative errors in the simulations. The SST_{skin} difference is related to the dust layer temperature; however, the aerosol concentration dominates the error. The aerosol dust introduced SST_{skin} errors reach about -14 K when the thick aerosol layer occurs at 3-4 km height, due to the relatively large temperature difference between the aerosol dust layer and the sea surface. The magnitudes of this negative SST_{skin} error are in broad agreement with those found in Bogdanoff et al. (2015) who investigated dust effects on AVHRR SST_{skin} retrievals.

To summarize the results of the RTTOV simulations to investigate the impact of aerosol dust on the SST_{skin}, the vertical distributions of aerosols influence the errors of infrared-derived SST_{skin}. The errors are greater for higher dust layers, because higher dust layers have a greater temperature difference to the sea surface. The magnitudes of the negative SST_{skin} errors can be as large as -14 K in the case of dense and high dust layers, occurring at 3-4 km height. On the other hand, a warm dust layer at lower altitudes can introduce a positive SST_{skin} retrieval error.

The results indicate that improvements in atmospheric correction algorithms to compensate for inaccuracies introduced by dust aerosol could be expected if efforts are made to take dust layer concentrations, altitudes and temperatures into account. This could be done by selecting coefficients in an NLSST-type algorithm that depend on prior information on aerosol conditions, or using such aerosol information in an optimal estimation approach (Merchant et al. 2008). Reliance on external aerosol information can be avoided by including additional aerosol-sensitive channels in the atmospheric correction algorithms (Luo et al. 2019; Merchant et al. 2006).

5. Summary

Instruments on the TERRA satellite provide a long-term, consistent and high-quality set of data records of the Earth system. SST_{skin}, as one of the mature products retrieved from MODIS onboard TERRA, has been developed and improved continually for many research and operational applications such as climate change studies and weather prediction. Although the MODIS onboard TERRA provides accurate estimates of the SST_{skin} fields, the residual uncertainty characteristics due to such atmospheric factors as aerosol dust cannot be ignored. This study aimed to improve the understanding of the effect of the vertical aerosol dust distribution on infrared satellite-derived SST_{skin}

by using match-up methods as well as radiative transfer simulations. High-accuracy shipboard derived SST_{skin}, using M-AERI, have been used to assess the aerosol dust effects. Radiosonde and M-AERI data collected within Saharan dust outflow regions during AEROSE cruises provide independent marine and atmospheric inputs for radiative transfer simulations. The key findings are summarized below.

The results from in-situ match-ups and radiative transfer simulations are comparable. Overall, the aerosol dust makes infrared SST_{skin} retrievals more negative; this is in agreement with the results of correction for MODIS (Luo et al. 2019) , and corrections for various sensors reported by other investigators (Blackmore et al. 2012; Bogdanoff et al. 2015; Good et al. 2012; Le Borgne et al. 2013; Merchant et al. 2006; Nalli et al. 2013). SST has been declared to be an Essential Climate Variable by the Global Observing System for Climate (GCOS; Bojinski et al. (2014)) with required measurement uncertainty of 0.1 K over 100 km scales (GCOS 2019). The SST_{skin} retrieval errors introduced by aerosol dust layers are significant in comparison to the requirements for the generation of SST Climate Data Records of an accuracy within 0.04 K per decade (Ohring et al. 2005). The variability in the thickness, altitudes and temperatures of dust layers can introduce additional uncertainties into comparisons between satellite- and M-AERI-derived SST_{skin}. As the aerosol altitude increases, the SST_{skin} difference becomes more negative, because higher dust layers have larger temperature contrasts to the sea surface. Saharan dust layers present in the lower troposphere are usually accompanied with high air temperatures, so the MODIS-derived SST_{skin} difference is likely to be positive. The SST_{skin} differences due to aerosol vertical distributions can vary with occasionally more extreme values between -3 K and 1 K.

Users seeking high-quality SSTs in areas where there is the risk of dust contamination are encouraged to pay attention to the Quality Level indicator of each pixel, and use the "best" quality data with QL=0. It should be noted that the MODIS R2019 reprocessed SST_{skin} retrievals include a correction for dust effects at night, as reported by Luo et al. (2019), but this correction does not take into account explicit dependences on altitude, and hence temperature, and dust concentration.

The MODIS NLSST does not use measurements from infrared channels with wavelengths close to 3.8 μm and 8.9 μm (GSFC 2020). As shown by Merchant et al. (2006) and other subsequent studies (Le Borgne et al. 2013; Luo et al. 2019), the off-axis characteristics of the brightness-temperature difference space of channels 20 (λ = 3.8 μm), 29 (λ = 8.9 μm), 31 (λ = 11 μm) and 32 (λ = 12 μm) can indicate the dust presence during nighttime and would be helpful to improve the SST_{skin} retrieval.

This study focused on MODIS onboard TERRA but since the MODIS onboard AQUA has consistent design and performance in terms of their spectral channels, calibration stability and other characterizations (Xiong et al. 2009; Xiong et al. 2008b), we expect similar results for Aqua MODIS SST_{skin} retrievals. Future work is planned to include a scheme to reduce the infrared satellites SST_{skin} errors by accounting for the vertical dust distribution. The measurements of aerosol vertical distributions and properties resolved by the lidar on the Cloud–Aerosol Lidar Infrared Pathfinder Satellite Observations (CALIPSO; Adams et al. (2012)) could be useful. Reanalysis data, such as those data from MERRA-2 and ECMWF ERA5 (Hersbach et al. 2020), can provide supplementary information when the CALIPSO data are not available. The solar and satellite zenith angles were set to zero in this study so other zenith angles dependences should be included in a future study. In the future, we may extend this study to newer sensors such as VIIRS and ABI. Also, mineral dust effects in other regions, such as at high latitudes where mineral dust lofted into the atmosphere (e.g. Dagsson-Waldhauserova et al. (2019); Vogelmann et al. (2003); Willis et al. (2018)), will be investigated.

Acknowledgments

This study was funded by Future Investigators in NASA Earth and Space Science and Technology (FINESST) Program grant 80NSSC19K1326. AEROSE is a collaboration with the NOAA PIRATA Northeast Extension (PNE) project and is supported by the NOAA Center for Atmospheric Sciences and Meteorology (NCAS-M) at Howard University (Prof. Vernon Morris, PI), the NOAA Educational Partnership Program grant NA17AE1625, NOAA grant NA17AE1623, the Joint Polar Satellite System (JPSS) and NOAA/NESDIS/STAR. The at-sea support of Malgorzata Szczodrak, Miguel Izaguirre and others is acknowledged, especially for deploying the radiosondes. The Officers, crew, and colleagues on the NOAA Ship *Ronald H Brown* and R/V *Alliance* are thanked for hosting M-AERI instruments. The thoughtful comments and suggestions of anonymous reviewers are acknowledged as these have led to an improved paper. Data files of MODIS L2P SST_{skin} and MERRA-2 fields were downloaded from the NASA PO.DAAC.

Credit authorship contribution statement:

Bingkun Luo: analysis; writing, review & editing; funding acquisition. Peter J. Minnett: supervision, writing, review & editing; Nicholas R. Nalli: analysis; data acquisition.

Declaration of competing interest:

The authors declare that they have no known competing financial interests or personal relationships that could have appeared to influence the work reported in this paper.

List of Figures

List of Tables

References

Adams, A.M., Prospero, J.M., & Zhang, C. (2012). CALIPSO-Derived Three-Dimensional Structure of Aerosol over the Atlantic Basin and Adjacent Continents. *Journal of Climate, 25*, 6862-6879. 10.1175/JCLI-D-11-00672.1

Adebiyi, A.A., Zuidema, P., & Abel, S.J. (2015). The convolution of dynamics and moisture with the presence of shortwave absorbing aerosols over the southeast Atlantic. *Journal of Climate, 28*, 1997-2024. https://doi.org/10.1175/JCLI-D-14-00352.1

Allison, L., & Kennedy, J. (1967). An Evaluation of Sea Surface Temperature as Measured by the Nimbus 1 High Resolution Infrared Radiometer. NASA Technical Note . Available at https://ntrs.nasa.gov/citations/19680000754

Arbelo, M., Podestá, G.P., Hernández-Leal, P.A., & Diaz, J.P. (2003). Use of TOMS data to correct the saharan dust effects on SST retrievals from satellite. *Advances in Space Research, 32*, 2175-2180. https://doi.org/10.1016/S0273-1177(03)90540-0

Bertie, J.E., & Lan, Z.D. (1996). Infrared intensities of liquids XX: the intensity of the OH stretching band revisited, and the best current values of the optical constants of H_2O (l) at 25ºC between 15,000 and 1 cm^{-1}. *App. Spectroscopy, 50*, 1047-1057. https://doi.org/10.1366/0003702963905385

Blackmore, T., O'Carroll, A., Fennig, K., & Saunders, R. (2012). Correction of AVHRR Pathfinder SST data for volcanic aerosol effects using ATSR SSTs and TOMS aerosol optical depth. *Remote Sensing of Environment, 116*, 107-117. https://doi.org/10.1016/j.rse.2011.04.040

Bogdanoff, A.S., Westphal, D.L., Campbell, J.R., Cummings, J.A., Hyer, E.J., Reid, J.S., & Clayson, C.A. (2015). Sensitivity of infrared sea surface temperature retrievals to the vertical distribution of airborne dust aerosol. *Remote Sensing of Environment, 159*, 1-13. http://dx.doi.org/10.1016/j.rse.2014.12.002

Bojinski, S., Verstraete, M., Peterson, T.C., Richter, C., Simmons, A., & Zemp, M. (2014). The Concept of Essential Climate Variables in Support of Climate Research, Applications, and Policy. *Bulletin of the American Meteorological Society, 95*, 1431-1443. 10.1175/bams-d-13-00047.1

Bosilovich, M.G., Santha, A., Lawrence, C., Richard, C., Clara, D., Ronald, G., Robin, K., Qing, L., Andrea, M., Peter, N., Krzysztof, W., Winston, C., Rolf, R., Lawrence, T., Yury, V., Steve, B., Allison, C., Stacey, F., Gordon, L., Gary, P., Steven, P., Oreste, R., Siegfried, D.S., & Max, S. (2015). MERRA-2: Initial Evaluation of the Climate. R.D. Koster. Technical Report Series on Global Modeling and Data Assimilation. pp 145. Greenbelt, Maryland 20771, USA. NASA Goddard Space Flight Center. Available at https://gmao.gsfc.nasa.gov/pubs/docs/Bosilovich803.pdf

Brasnett, B. (2008). The impact of satellite retrievals in a global sea-surface-temperature analysis. *Quarterly Journal of the Royal Meteorological Society, 134*, 1745-1760. https://doi.org/10.1002/qj.319

Brown, O.B., & Minnett, P.J. (1999). MODIS Infrared Sea Surface Temperature Algorithm Theoretical Basis Document, Version 2.0. pp 98. Available at http://oceancolor.gsfc.nasa.gov/cmsdocs/technical_documents/atbd_mod25.pdf

Brown, S.J., Harris, A.R., Mason, I.M., & Závody, A.M. (1997). New aerosol robust sea surface temperature algorithms for the along-track scanning radiometer. *Journal of Geophysical Research, 102*, 27,973–927,989. doi: 10.1029/97JC01192

Buchard, V., Randles, C.A., da Silva, A.M., Darmenov, A., Colarco, P.R., Govindaraju, R., Ferrare, R., Hair, J., Beyersdorf, A.J., Ziemba, L.D., & Yu, H. (2017). The MERRA-2 Aerosol Reanalysis, 1980 Onward. Part II: Evaluation and Case Studies. *Journal of Climate, 30*, 6851-6872. 10.1175/jcli-d-16-0613.1

Carlson, T.N., & Benjamin, S.G. (1980). Radiative heating rates for Saharan dust. *Journal of the Atmospheric Sciences, 37*, 193-213. https://doi.org/10.1175/1520-0469(1980)037%3C0193:RHRFSD%3E2.0.CO;2

Choobari, O.A., Zawar-Reza, P., & Sturman, A. (2014). The global distribution of mineral dust and its impacts on the climate system: A review. *Atmospheric Research, 138*, 152-165. https://doi.org/10.1016/j.atmosres.2013.11.007

Cracknell, A.P. (1997). *The Advanced Very High Resolution Radiometer*. London, UK: CRC Press, Taylor and Francis

Dagsson-Waldhauserova, P., Renard, J.-B., Olafsson, H., Vignelles, D., Berthet, G., Verdier, N., & Duverger, V. (2019). Vertical distribution of aerosols in dust storms during the Arctic winter. *Scientific Reports, 9*, 16122. 10.1038/s41598-019-51764-y

Díaz, J.P., Arbelo, M., Expósito, F.J., Podestá, G., Prospero, J.M., & Evans., R. (2001). Relationship between errors in AVHRR-derived sea surface temperature and the TOMS Aerosol Index. *Geophysical Research Letters, 28*, 1989–1992. https://doi.org/10.1029/2000GL012446

Donlon, C., Berruti, B., Buongiorno, A., Ferreira, M.H., Féménias, P., Frerick, J., Goryl, P., Klein, U., Laur, H., Mavrocordatos, C., Nieke, J., Rebhan, H., Seitz, B., Stroede, J., & Sciarra, R. (2012). The Global Monitoring for Environment and Security (GMES) Sentinel-3 mission. *Remote Sensing of Environment, 120*, 37-57. 10.1016/j.rse.2011.07.024

Donlon, C.J., Minnett, P.J., Fox, N., & Wimmer, W. (2014a). Strategies for the Laboratory and Field Deployment of Ship-Borne Fiducial Reference Thermal Infrared Radiometers in Support of Satellite-Derived Sea Surface Temperature Climate Data Records. In G. Zibordi, C.J. Donlon, & A.C. Parr (Eds.), *Experimental Methods in the Physical Sciences, Vol 47, Optical Radiometry for Ocean Climate Measurements* (pp. 557-603): Academic Press

Donlon, C.J., Minnett, P.J., Jessup, A., Barton, I., Emery, W., Hook, S., Wimmer, W., Nightingale, T.J., & Zappa, C. (2014b). Ship-Borne Thermal Infrared Radiometer Systems. In G. Zibordi, C.J. Donlon, & A.C. Parr (Eds.), *Experimental Methods in the Physical Sciences, Vol 47, Optical Radiometry for Ocean Climate Measurements* (pp. 305-404): Academic Press

Donlon, C.J., Robinson, I., Casey, K.S., Vazquez-Cuervo, J., Armstrong, E., Arino, O., Gentemann, C., May, D., LeBorgne, P., Piollé, J., Barton, I., Beggs, H., Poulter, D.J.S., Merchant, C.J., Bingham, A., Heinz, S., Harris, A., Wick, G., Emery, B., Minnett, P., Evans, R., Llewellyn-Jones, D., Mutlow, C., Reynolds, R.W., Kawamura, H., & Rayner, N. (2007). The Global Ocean Data Assimilation Experiment High-resolution Sea Surface Temperature Pilot Project. *Bulletin of the American Meteorological Society, 88*, 1197-1213. https://doi.org/10.1175/BAMS-88-8-1197

Downing, H.D., & Williams, W. (1975). Optical constants of water in the infrared. *J. Geophys. Res. 80, 1656-1661.*https://doi.org/10.1029/JC080i012p01656

Embury, O., & Merchant, C.J. (2012). A reprocessing for climate of sea surface temperature from the along-track scanning radiometers: A new retrieval scheme. *Remote Sensing of Environment, 116*, 47-61. 10.1016/j.rse.2010.11.020
Embury, O., Merchant, C.J., & Filipiak, M.J. (2012). A reprocessing for climate of sea surface temperature from the along-track scanning radiometers: Basis in radiative transfer. *Remote Sensing of Environment, 116*, 32-46. 10.1016/j.rse.2010.10.016
Esaias, W.E., Abbott, M.R., Barton, I., Brown, O.B., Campbell, J.W., Carder, K.L., Clark, D.K., Evans, R.H., Hoge, F.E., Gordon, H.R., Balch, W.M., Letelier, R., & Minnett., P.J. (1998). An Overview of MODIS Capabilities for Ocean Science Observations. *IEEE Transactions on Geoscience and Remote Sensing, 36*, 1250-1265. https://doi.org/10.1109/36.701076
Fowler, J.B. (1995). A third generation water bath based blackbody source. *Journal of Research of the National Institute of Standards and Technology, 100*, 591-599. 10.6028/jres.100.044
GCOS. (2019). Sea Surface Temperature ESSENTIAL CLIMATE VARIABLE (ECV) FACTSHEET. WMO. Available at https://ane4bf-datap1.s3.eu-west-1.amazonaws.com/wmod8_climatedata/s3fs-public/sea_surface_temp_ecv_factsheet_20190129.pdf?S1Ytg0lpZBI305EokCRPqHi_XU4TP_Db
Gelaro, R., McCarty, W., Suárez, M.J., Todling, R., Molod, A., Takacs, L., Randles, C.A., Darmenov, A., Bosilovich, M.G., Reichle, R., Wargan, K., Coy, L., Cullather, R., Draper, C., Akella, S., Buchard, V., Conaty, A., da Silva, A.M., Gu, W., Kim, G.-K., Koster, R., Lucchesi, R., Merkova, D., Nielsen, J.E., Partyka, G., Pawson, S., Putman, W., Rienecker, M., Schubert, S.D., Sienkiewicz, M., & Zhao, B. (2017). The Modern-Era Retrospective Analysis for Research and Applications, Version 2 (MERRA-2). *Journal of Climate, 30*, 5419-5454. 10.1175/jcli-d-16-0758.1
Gentemann, C.L., Minnett, P.J., & Ward, B. (2009). Profiles of Ocean Surface Heating (POSH): a new model of upper ocean diurnal thermal variability. *Journal of Geophysical Research, 114*, C07017. 10.1029/2008JC004825
Good, E.J., Kong, X., Embury, O., Merchant, C.J., & Remedios, J.J. (2012). An infrared desert dust index for the Along-Track Scanning Radiometers. *Remote Sensing of Environment, 116*, 159-176. 10.1016/j.rse.2010.06.016
GSFC. (2020). Sea Surface Temperature (SST) R2019 Algorithm Theoretical Basis Documents. Available at https://oceancolor.gsfc.nasa.gov/atbd/sst/
Hale, G.M., & Querry, M.R. (1973). Optical Constants of Water in the 200-nm to 200-μm Wavelength Region. *Applied Optics, 12*, 555-563. 10.1364/AO.12.000555
Hansell, R., Tsay, S., Ji, Q., Hsu, N., Jeong, M., Wang, S., Reid, J., Liou, K., & Ou, S. (2010). An assessment of the surface longwave direct radiative effect of airborne Saharan dust during the NAMMA field campaign. *Journal of the Atmospheric Sciences, 67*, 1048-1065. https://doi.org/10.1175/2009JAS3257.1
Haywood, J.M., Allan, R.P., Culverwell, I., Slingo, T., Milton, S., Edwards, J., & Clerbaux, N. (2005). Can desert dust explain the outgoing longwave radiation anomaly over the Sahara during July 2003? *Journal of Geophysical Research, 110*, D05105. https://doi.org/10.1029/2004JD005232
Hersbach, H., Bell, B., Berrisford, P., Hirahara, S., Horányi, A., Muñoz-Sabater, J., Nicolas, J., Peubey, C., Radu, R., Schepers, D., Simmons, A., Soci, C., Abdalla, S.,

Abellan, X., Balsamo, G., Bechtold, P., Biavati, G., Bidlot, J., Bonavita, M., De Chiara, G., Dahlgren, P., Dee, D., Diamantakis, M., Dragani, R., Flemming, J., Forbes, R., Fuentes, M., Geer, A., Haimberger, L., Healy, S., Hogan, R.J., Hólm, E., Janisková, M., Keeley, S., Laloyaux, P., Lopez, P., Lupu, C., Radnoti, G., de Rosnay, P., Rozum, I., Vamborg, F., Villaume, S., & Thépaut, J.-N. (2020). The ERA5 global reanalysis. *Quarterly Journal of the Royal Meteorological Society*https://doi.org/10.1002/qj.3803

Hess, M., Koepke, P., & Schult, I. (1998). Optical properties of aerosols and clouds: The software package OPAC. *Bulletin of the American Meteorological Society, 79*, 831-844. https://doi.org/10.1175/1520-0477(1998)079%3C0831:OPOAAC%3E2.0.CO;2

Judd, K.P., & Handler, R.A. (2019). Numerical Solution of the Radiation Transport Equation at an Air-Water Interface for a Stratified Medium. *Frontiers in Mechanical Engineering, 5*, 1. https://doi.org/10.3389/fmech.2019.00001

Karyampudi, V.M., Palm, S.P., Reagen, J.A., Fang, H., Grant, W.B., Hoff, R.M., Moulin, C., Pierce, H.F., Torres, O., Browell, E.V., & Melfi, S.H. (1999). Validation of the Saharan Dust Plume Conceptual Model Using Lidar, Meteosat, and ECMWF Data. *Bulletin of the American Meteorological Society, 80*, 1045-1076. 10.1175/1520-0477(1999)080<1045:Votsdp>2.0.Co;2

Kilpatrick, K.A., Podestá, G., Walsh, S., Williams, E., Halliwell, V., Szczodrak, M., Brown, O.B., Minnett, P.J., & Evans, R. (2015). A decade of sea surface temperature from MODIS. *Remote Sensing of Environment, 165*, 27-41. http://dx.doi.org/10.1016/j.rse.2015.04.023

Kilpatrick, K.A., Podestá, G., Williams, E., Walsh, S., & Minnett, P.J. (2019). Alternating Decision Trees for Cloud Masking in MODIS and VIIRS NASA Sea Surface Temperature Products. *Journal of Atmospheric and Oceanic Technology, 36*, 387-407. https://doi.org/10.1175/JTECH-D-18-0103.1

Kilpatrick, K.A., Podestá, G.P., & Evans, R.H. (2001). Overview of the NOAA/NASA Pathfinder algorithm for Sea Surface Temperature and associated Matchup Database. *Journal of Geophysical Research, 106*, 9179-9198. https://doi.org/10.1029/1999JC000065

Le Borgne, P., Péré, S., & Roquet, H. (2013). Night time detection of Saharan dust using infrared window channels: Application to NPP/VIIRS. *Remote Sensing of Environment, 137*, 264-273. https://doi.org/10.1016/j.rse.2013.06.001

Luo, B., & Minnett, P. (2020). Evaluation of the ERA5 Sea Surface Skin Temperature with Remotely-Sensed Shipborne Marine-Atmospheric Emitted Radiance Interferometer Data. *Remote Sensing, 12*, 1873. doi:10.3390/rs12111873

Luo, B., Minnett, P.J., Gentemann, C., & Szczodrak, G. (2019). Improving satellite retrieved night-time infrared sea surface temperatures in aerosol contaminated regions. *Remote Sensing of Environment, 223*, 8-20. https://doi.org/10.1016/j.rse.2019.01.009

Luo, B., Minnett, P.J., Szczodrak, M., Kilpatrick, K., & Izaguirre, M. (2020a). Validation of Sentinel-3A SLSTR derived Sea-Surface Skin Temperatures with those of the shipborne M-AERI. *Remote Sensing of Environment, 244*, 111826. https://doi.org/10.1016/j.rse.2020.111826

Luo, B., Minnett, P.J., Szczodrak, M., Nalli, N.R., & Morris, V.R. (2020b). Accuracy assessment of MERRA-2 and ERA-Interim sea-surface temperature, air temperature and humidity profiles over the Atlantic Ocean using AEROSE measurements. *Journal of Climate, 33*, 6889–6909. 10.1175/JCLI-D-19-0955.1

Marullo, S., Santoleri, R., Banzon, V., Evans, R.H., & Guarracino, M. (2010). A diurnal-cycle resolving sea surface temperature product for the tropical Atlantic. *Journal of Geophysical Research: Oceans, 115*, C05011. 10.1029/2009JC005466
McCarty, W., Coy, L., Gelaro, R., Huang, A., Merkova, D., Smith, E.B., Sienkiewicz, M., & Wargan, K. (2016). MERRA-2 Input Observations: Summary and Assessment. Technical Report Series on Global Modeling and Data Assimilation. Volume 46. Available at https://gmao.gsfc.nasa.gov/pubs/docs/McCarty885.pdf. NASA/TM–2016-104606/Vol. 46
McClatchey, R.A. (1972). *Optical properties of the atmosphere*. Air Force Cambridge Research Laboratories, Office of Aerospace Research
Merchant, C. (2012). SENTINEL-3 Sea Surface Temperature (SLSTR) Algorithm Theoretical Basis Document. In. EUMETSAT https://www.eumetsat.int/website/wcm/idc/idcplg?IdcService=GET_FILE&dDocName=PDF_S3_L2_ATBD_SLSTR_SST&RevisionSelectionMethod=LatestReleased&Rendition=Web: University of Edinburgh
Merchant, C.J., Embury, O., Bulgin, C.E., Block, T., Corlett, G.K., Fiedler, E., Good, S.A., Mittaz, J., Rayner, N.A., & Berry, D. (2019). Satellite-based time-series of sea-surface temperature since 1981 for climate applications. *Scientific data, 6*, 1-18.
Merchant, C.J., Embury, O., Le Borgne, P., & Bellec, B. (2006). Saharan dust in nighttime thermal imagery: Detection and reduction of related biases in retrieved sea surface temperature. *Remote Sensing of Environment, 104*, 15-30.
Merchant, C.J., Harris, A.R., Maturi, E., & MacCallum, S. (2005). Probabilistic physically based cloud screening of satellite infrared imagery for operational sea surface temperature retrieval. *Quarterly Journal of the Royal Meteorological Society, 131*, 2735–2755. doi: 10.1256/qj.05.15
Merchant, C.J., LeBorgne, P., Marsouin, A., & Roquet, H. (2008). Optimal estimation of sea surface temperature from split-window observations. *Remote Sensing of Environment, 112*, 2469-2484. https://doi.org/10.1016/j.rse.2007.11.011
Minnett, P.J. (2003). Radiometric measurements of the sea-surface skin temperature - the competing roles of the diurnal thermocline and the cool skin. *International Journal of Remote Sensing, 24*, 5033-5047. https://doi.org/10.1080/0143116031000095880
Minnett, P.J., Alvera-Azcárate, A., Chin, T.M., Corlett, G.K., Gentemann, C.L., Karagali, I., Li, X., Marsouin, A., Marullo, S., Maturi, E., Santoleri, R., Saux Picart, S., Steele, M., & Vazquez-Cuervo, J. (2019). Half a century of satellite remote sensing of sea-surface temperature. *Remote Sensing of Environment, 233*, 111366. https://doi.org/10.1016/j.rse.2019.111366
Minnett, P.J., & Kaiser-Weiss, A.K. (2012). Group for High Resolution Sea-Surface Temperature Discussion Document: Near-Surface Oceanic Temperature Gradients.. Available at https://www.ghrsst.org/wp-content/uploads/2016/10/SSTDefinitionsDiscussion.pdf
Minnett, P.J., Kilpatrick, K., Podestá, G., Evans, R.H., Szczodrak, M., Izaguirre, M.A., Williams, E., Walsh, S., Reynolds, R.M., Bailey, S.W., Armstrong, E.M., & Vazquez-Cuervo, J. (2020). Skin Sea-Surface Temperature from VIIRS on Suomi-NPP – NASA Continuity Retrievals. *Remote Sensing, In review*
Minnett, P.J., Knuteson, R.O., Best, F.A., Osborne, B.J., Hanafin, J.A., & Brown, O.B. (2001). The Marine-Atmospheric Emitted Radiance Interferometer (M-AERI), a high-

accuracy, sea-going infrared spectroradiometer. *Journal of Atmospheric and Oceanic Technology, 18*, 994-1013. https://doi.org/10.1175/1520-0426(2001)018%3C0994:TMAERI%3E2.0.CO;2
Morris, V., Clemente-Colón, P., Nalli, N.R., E. Joseph, R. A. Armstrong, Y. Detrés, M. D. Goldberg, Minnett, P.J., & Lumpkin, R. (2006). Measuring Trans-Atlantic Aerosol Transport From Africa. *EOS, Transactions of the American Geophysical Union, 87*, 565,571. https://doi.org/10.1029/2006EO500001
Nalli, N.R., Barnet, C.D., Gambacorta, A., Maddy, E.S., Xie, H., King, T.S., Joseph, E., & Morris, V.R. (2013). On the angular effect of residual clouds and aerosols in clear-sky infrared window radiance observations 2. Satellite experimental analyses. *Journal of Geophysical Research: Atmospheres, 118*, 1420-1435. 10.1029/2012jd018260
Nalli, N.R., Barnet, C.D., Maddy, E.S., & Gambacorta, A. (2012). On the angular effect of residual clouds and aerosols in clear-sky infrared window radiance observations: Sensitivity analyses. *Journal of Geophysical Research: Atmospheres, 117*https://doi.org/10.1029/2012JD017667
Nalli, N.R., Joseph, E., Morris, V.R., Barnet, C.D., Wolf, W.W., Wolfe, D., Minnett, P.J., Szczodrak, M., Izaguirre, M.A., Lumpkin, R., Xie, H., Smirnov, A., King, T.S., & Wei, J. (2011). Multiyear Observations of the Tropical Atlantic Atmosphere: Multidisciplinary Applications of the NOAA Aerosols and Ocean Science Expeditions. *Bulletin of the American Meteorological Society, 92*, 765-789. 10.1175/2011BAMS2997.1
Nalli, N.R., & Stowe, L.L. (2002). Aerosol correction for remotely sensed sea surface temperatures from the National Oceanic and Atmospheric Administration advanced very high resolution radiometer. *Journal of Geophysical Research, 107*doi:10.1029/2001JC001162
O'Carroll, A.G., Blackmore, T., Fennig, K., Saunders, R.W., & Millington, S. (2012). Towards a bias correction of the AVHRR Pathfinder SST data from 1985 to 1998 using ATSR. *Remote Sensing of Environment, 116*, 118-125. 10.1016/j.rse.2011.05.023
Ohring, G., Wielicki, B., Spencer, R., Emery, B., & Datla, R. (2005). Satellite Instrument Calibration for Measuring Global Climate Change: Report of a Workshop. *Bulletin of the American Meteorological Society, 86*, 1303-1313. https://doi.org/10.1175/BAMS-86-9-1303
Randles, C.A., Da Silva, A.M., Buchard, V., Colarco, P.R., Darmenov, A., Govindaraju, R., Smirnov, A., Holben, B., Ferrare, R., Hair, J., Shinozuka, Y., & Flynn, C.J. (2017). The MERRA-2 Aerosol Reanalysis, 1980 - onward, Part I: System Description and Data Assimilation Evaluation. *J Clim, 30*, 6823-6850. 10.1175/JCLI-D-16-0609.1
Reynolds, R.W., & Smith, T.M. (1994). Improved global sea surface temperature analysis using optimum interpolation. *J. Climate, 7*, 929-948. https://doi.org/10.1175/1520-0442(1994)007%3C0929:IGSSTA%3E2.0.CO;2
Rice, J.P., Butler, J.J., Johnson, B.C., Minnett, P.J., Maillet, K.A., Nightingale, T.J., Hook, S.J., Abtahi, A., Donlon, C.J., & Barton, I.J. (2004). The Miami2001 Infrared Radiometer Calibration and Intercomparison: 1. Laboratory Characterization of Blackbody Targets. *Journal of Atmospheric and Oceanic Technology, 21*, 258-267. https://doi.org/10.1175/1520-0426(2004)021%3C0268:TMIRCA%3E2.0.CO;2
Saunders, R., Hocking, J., Turner, E., Rayer, P., Rundle, D., Brunel, P., Vidot, J., Roquet, P., Matricardi, M., & Geer, A. (2018). An update on the RTTOV fast radiative transfer

model (currently at version 12). *Geoscientific Model Development, 11*https://doi.org/10.5194/gmd-11-2717-2018
Schmülling, F., Zerfowski, I., Pillukat, A., & Bonsignori, R. (2010). METimage: a multispectral imaging radiometer for the EUMETSAT Polar System follow-on satellite mission. In, *SPIE Remote Sensing - SPIE 7826, Sensors, Systems, and Next-Generation Satellites XIV* (p. 7). Toulouse, France: SPIE
Schueler, C.F., Lee, T.F., & Miller, S.D. (2013). VIIRS constant spatial-resolution advantages. *International Journal of Remote Sensing, 34*, 5761-5777. 10.1080/01431161.2013.796102
Smith, W.L., Knuteson, R.O., Revercomb, H.E., Feltz, W., Howell, H.B., Menzel, W.P., Nalli, N., Brown, O., Brown, J., Minnett, P., & McKeown, W. (1996). Observations of the infrared radiative properties of the ocean - implications for the measurement of sea surface temperature via satellite remote sensing. *Bulletin of the American Meteorological Society, 77*, 41-51. https://doi.org/10.1175/1520-0477(1996)077%3C0041:OOTIRP%3E2.0.CO;2
Smith, W.L., Rao, P.K., Koffler, R., & Curtis, W. (1970). The determination of sea-surface temperature from satellite high resolution infrared window radiation measurements. *Monthly Weather Review, 98*, 604-611. https://doi.org/10.1175/1520-0493(1970)098%3C0604:TDOSST%3E2.3.CO;2
Szczodrak, M., Minnett, P.J., & Evans, R.H. (2014). The effects of anomalous atmospheres on the accuracy of infrared sea-surface temperature retrievals: Dry air layer intrusions over the tropical ocean. *Remote Sensing of Environment, 140*, 450-465. http://dx.doi.org/10.1016/j.rse.2013.09.010
Theocharous, E., Fox, N., Barker-Snook, I., Niclòs, R., Santos, V.G., Minnett, P.J., Göttsche, F., Poutier, L., Morgan, N., & Nightingale, T. (2019). The 2016 CEOS infrared radiometer comparison: Part II: laboratory comparison of radiation thermometers. *Journal of Atmospheric and Oceanic Technology, 36*, 1079-1092. https://doi.org/10.1175/JTECH-D-18-0032.1
Twomey, S. (1972). The effect of cloud scattering on the absorption of solar radiation by atmospheric dust. *Journal of the Atmospheric Sciences, 29*, 1156-1159. https://doi.org/10.1175/1520-0469(1972)029%3C1156:TEOCSO%3E2.0.CO;2
Vázquez-Cuervo, J., Armstrong, E., & Harris, A. (2004). The effect of Aerosols and Clouds on the Retrieval of Infrared Sea Surface Temperatures. *Journal of Climate, 17*, 3921-3933. https://doi.org/10.1175/1520-0442(2004)017%3C3921:TEOAAC%3E2.0.CO;2
Vogelmann, A.M., Flatau, P.J., M.Szczodrak, Markowicz, K., & Minnett., P.J. (2003). Observations of Large Aerosol Infrared Forcing at the Surface. *Geophysical Research Letters, 30*, 1655.
Wallner, O., Reinert, T., & Straif, C. (2017). METIMAGE: a spectro-radiometer for the VII mission onboard METOP-SG. In, *In Proceedings of International Conference on Space Optics — ICSO 2016, Biarritz, France, Bruno Cugny, Nikos Karafolas and Zoran Sodnik (Eds.)* (p. 8): SPIE
Walton, C., Pichel, W., Sapper, J., & May, D. (1998). The development and operational application of nonlinear algorithms for the measurement of sea surface temperatures with the NOAA polar‐orbiting environmental satellites. *Journal of Geophysical Research: Oceans, 103*, 27999-28012. https://doi.org/10.1029/98JC02370

Walton, C.C. (2016). A review of differential absorption algorithms utilized at NOAA for measuring sea surface temperature with satellite radiometers. *Remote Sensing of Environment, 187*, 434-446. http://dx.doi.org/10.1016/j.rse.2016.10.011
Weaver, C.J., Ginoux, P., Hsu, N.C., Chou, M.-D., & Joiner, J. (2002). Radiative forcing of Saharan dust: GOCART model simulations compared with ERBE data. *Journal of the Atmospheric Sciences, 59*, 736-747. https://doi.org/10.1175/1520-0469(2002)059%3C0736:RFOSDG%3E2.0.CO;2
Willis, M.D., Leaitch, W.R., & Abbatt, J.P.D. (2018). Processes Controlling the Composition and Abundance of Arctic Aerosol. *Reviews of Geophysics, 56*, 621-671. 10.1029/2018rg000602
Wong, S., Dessler, A.E., Mahowald, N.M., Yang, P., & Feng, Q. (2009). Maintenance of lower tropospheric temperature inversion in the Saharan air layer by dust and dry anomaly. *Journal of Climate, 22*, 5149-5162. https://doi.org/10.1175/2009JCLI2847.1
Xiong, X., Chiang, K., Wu, A., Barnes, W.L., Guenther, B., & Salomonson, V.V. (2008a). Multiyear On-Orbit Calibration and Performance of Terra MODIS Thermal Emissive Bands. *IEEE Transactions on Geoscience and Remote Sensing, 46*, 1790-1803. 10.1109/TGRS.2008.916217
Xiong, X., Wenny, B.N., & Barnes, W.D. (2009). Overview of NASA Earth Observing Systems Terra and Aqua moderate resolution imaging spectroradiometer instrument calibration algorithms and on-orbit performance. *Journal of Applied Remote Sensing, 3*, 032501. https://doi.org/10.1117/1.3180864
Xiong, X., Wu, A., & Cao, C. (2008b). On‐orbit calibration and inter‐comparison of Terra and Aqua MODIS surface temperature spectral bands. *International Journal of Remote Sensing, 29*, 5347-5359. https://doi.org/10.1080/01431160802036300